MODELING THE POTENTIAL USE OF POLYFLUORINATED PHTHALOCYANINES AS PHOTOSENSITIZERS IN PHOTODYNAMIC THERAPY

by

Başak Koca

B.S., Chemistry, Istanbul Technical University, 2016

Submitted to the Institute for Graduate Studies in
Science and Engineering in partial fulfillment of
the requirements for the degree of
Master of Science

Graduate Program in Chemistry
Boğaziçi University
2019

ACKNOWLEDGEMENTS

First and foremost, my deepest graditude goes to my advisor, Prof. Viktorya Aviyente, for her advice, encouragement, understanding, continuous support and patience. I would like to thank my thesis supervisor, Assoc. Prof. Şaron Çatak for her guidance and comments. I have gained valuable information and experience from them.

I wish to extend my appreciation to my thesis committee members: Assist. Prof. Oktay Demircan and my bachelor degree advisor, Prof. Esin Hamuryudan. I would also like to thank her for sharing her research for my master thesis.

I am gratefully acknowledge Assoc. Prof. Antonio Monari for his enlightening feedbacks, comments and questions that have offered alternative approaches to the study. I am also thankful for hosting me in Theory-Modeling-Simulation Lab, in Nancy.

I thank all the current and former members of CCBG lab for their friendship. Especially, I would like to thank my dear friends Deniz Akgül, İpek Munar, Semiha K. Bali and Evrim Arslan for creating warm environment in KB 332A. Our coffee breaks were full of laugh, science, linux, chitchat and joy.

My sister from another mother, Ayşenur Karaman, thank you for being in every stage of my university life. Without our limitless gossip capability, serious discussions, fun talks, this thesis would hardly been written. My cousin-like friend, Erberk Alpan, when I am in trouble, you are always there. You both showed me that friends are the family that we choose for ourselves.

Volkan Fındık, thank you for being my full-time supporter as well as my superhero. You have been always trying to encourage and motivate me to progress and move forward. You have done a lot for me and I am really lucky to have you, by my side.

Finally, I wish to thank my parents, Sedat Koca and Ayşe Koca, to whom I am indebted for their endless support and the understanding they have shown thoughout. You brighten up my life with your presence and I dedicate my dissertation study to both of you.

ABSTRACT

MODELING THE POTENTIAL USE OF POLYFLUORINATED PHTHALOCYANINES AS PHOTOSENSITIZERS IN PHOTODYNAMIC THERAPY

In recent years, phthalocyanine compounds which possess an aromatic macrocyclic ring, have been extensively used in photodynamic therapy as non-toxic photosensitizers due to their photophysical properties and their intense absorption in the near infrared region of the visible spectrum. However, there may be predominant factors such as metal ion, substituent effects that enhance the efficiency of phthalocyanines as photosensitizers and they have considerable influence on the excited state properties, electronic spectra, intersystem crossing probability. They ultimately determine the phthalocyanine propensity to activate the singlet oxygen which is held responsible for cell death. A theoretical evaluation of photophysical properties could give preliminary hints about the singlet oxygen generation ability. In this study, Density Functional Theory (DFT) and Time Dependent Density Functional Theory (TDDFT) at ωB97XD/6-311G**//B3LYP/6-31G* level of theory has been used to elucidate the optical properties of pentafluorobenzyloxy- substituted phthalocyanines as well as of their unsubstituted analogues. To achieve the dynamic effects in absorption and emission spectra, Wigner Distribution has been used by sampling the excited state and ground state geometries.

ÖZET

FOTODİNAMİK TERAPİDE KULLANIM POTANSİYELİ OLAN FLORLU FTALOSİYANİN TÜREVLERİNİN MODELLENMESİ

Son yıllarda, aromatik makrosiklik halka içeren ftalosiyanin bileşikleri, fotofiziksel özellikleri ve görünür ışık görüngesinde yakın kırmızı bölgede verdiği yüksek soğurma nedeniyle fotodinamik terapi adı verilen tedavide toksik olmayan fotoalgılayıcı ilaç olarak yaygın bir şekilde kullanılmaktadır. Ancak, ftalosiyaninin fotoalgılayıcı ajan olarak etkiniğini arttırabilecek metal iyonu, substituent etkisi gibi etkenler olabilir. Bu etkenlerin büyük ölçüde uyarılmış hal özelliklerine, ve bunun sonuncunda, ftalosiyaninin hücrelerin tahribatından sorumlu singlet oksijeninin aktivasyonuna eğilimini de etkilemektedirler. Fotofiziksel özelliklerin teorik incelenmesi singlet oksijen meydana getirme becerisi hakkında ön ipucu elde edilmesini sağlayabilir. Bu çalışmada, ωB97XD/6-311G**//B3LYP/6-31G* teorisi seviyesinde Yoğunluk Fonksiyonel Teorisi ve Zamana Bağımlı Yoğunluk Fonksiyonel Teorisi kullanılarak, pentaflorobenziloksi- substitüe ve onlarin sübstitüentsiz versiyonlarının optik özellikleri incelenmiştir. Dinamik etkilerin dahil olduğu soğurma ve yayınım spektrumlarını elde edebilmek için, temel hal ve uyarılmış hal geometrilerinden örnekler alınarak Wigner Dağılımı kullanılmıştır.

TABLE OF CONTENTS

LIST OF FIGURES

LIST OF TABLES

LIST OF SYMBOLS

E_{el}	Electronic Energy
$\mathrm{E}_{\mathrm{c}}[\rho]$	Correlation Energy
$\mathrm{E}_{\mathrm{x}}[\rho]$	Exchange Energy
H	Hamiltonian Operator
h_{KS}	Kohn-Sham Hamiltonian Operator
$\mathrm{J}[\rho(\mathrm{r})]$	Coulomb Energy
$\mathrm{T}[\rho(r)]$	Kinetic Energy of Interacting Electrons
$\mathrm{T}_{ni}[\rho(r)]$	Kinetic Energy of Non-Interacting Electrons
$V_{ext}(r)$	External Potential
$V_{ee}[\rho(r)]$	Electron-Electron Interactions
Z	Atomic Number
Δ_{ST}	Singlet-Triplet Gap
$\rho(\mathrm{r})$	Electron Density
ψ_i	Kohn-Sham Orbitals
ϕ_s	Quantitative Topological Descriptor
Γ	Detachment Density Matrix
Λ	Attachment Density Matrix
Ψ	Wavefunction

LIST OF ACRONYMS/ABBREVIATIONS

ADF	Amsterdam Density Functional
B3LYP	Becke-3-parameter Lee-Yang-Par functional
DFT	Density Functional Theory
DFA	Density Functional Approximation
EWG	Electron Withdrawing Group
GGA	Generalized Gradient Approximation
GTO	Gaussian Type Orbital
H_2Pc	Metal-Free Phthalocyanine
HF	Hartree-Fock theory
HOMO	Highest Occupied Molecular Orbital
IC	Internal Conversion
NIR	Near-Infrared Region
ISC	Intersystem Crossing
LC	Long-range Corrected
LCAO	Linear Combination of Atomic Orbitals
LDA	Local Density Approximation
LUMO	Lowest Unoccupied Molecular Orbital
MPc	Metallophthalocyanine
oNTO	Occupied Natural Transition Orbital
PCM	Polarizable Continuum Model
Pc	Phthalocyanine
PDT	Photodynamic Therapy
PS	Photosensitizer
SOC	Spin-Orbit Coupling
SOCC	Spin-Orbit Coupling Constant
STO	Slater Type Orbital
TD-DFT	Time Dependent Density Functional Theory
vNTO	Virtual Natural Transition Orbital

WDF	Wigner Distribution Function
WVD	Wigner-Ville Distribution
XC	Exchange-Correlation
ωB97xD	Long-Range Corrected Hybrid Functional with Dispersion Correction

1. INTRODUCTION

1.1. Tetrapyrrole Compounds

Macrocyclic compounds are at least 9 membered rings that have 3 atoms different from the carbon atom. Heteroatoms within this ring can be nitrogen, oxygen or sulphur atom. In 1967, C.J. Pedersen published a study on the crown ethers which was an important development in the field of coordination chemistry of macrocyclic compounds [1]. Today, there are several examples of macrocyclic compounds; some of them are crown ethers, cryptands, calixarenes and tetrapyrrole derivatives.

The macrocyclic tetrapyrrole derivatives comprise the porphyrins and their analogues which are porphyrazines, tetrabenzoporphyrins and phthalocyanines as seen in Figure 1.1. Basically, they contain 4 pyrrole or pyrrole-like rings which are interconnected through their α-carbons via aza bridges or methine bridges.

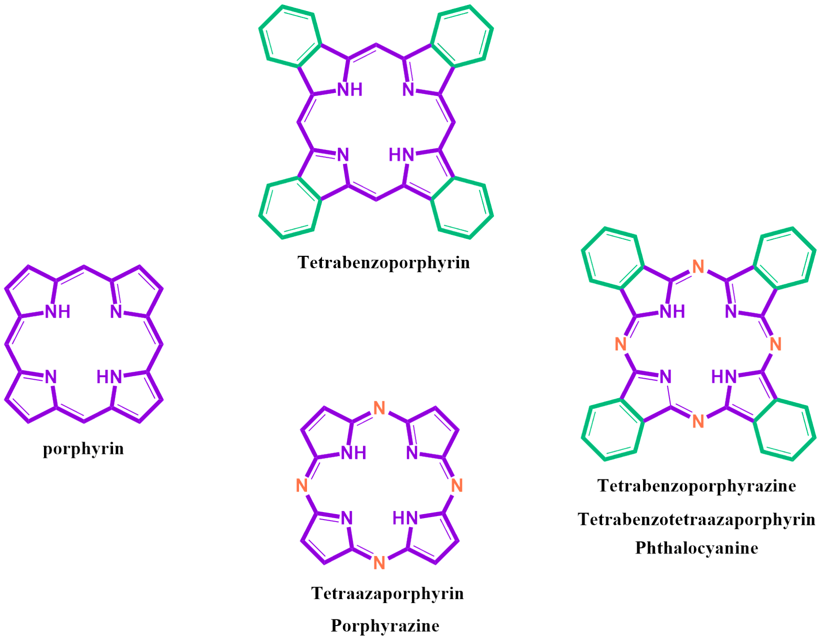

Figure 1.1. Structures of tetrapyrrole derivatives.

Among the tetrapyrrole derivatives, the porphyrins naturally exist in biological systems. Cytochrome is the heme-containing protein and the heme, an iron coordinated porphyrin complex carries the oxygen to the living cells [2]. The chemical structure of chlorophyll, vital part of green plants, is a porphyrin-like heterocycle. Since these macrocycles exhibit unique physical, chemical and spectral properties, they extensively play a part in nature and in several application area. Similarly, porphyrazines and phthalocyanines are synthetic macrocycles.

The most important features of tetrapyrrole derivatives are their planar structure and aromacity. These compounds include conjugated double bonds and along the conjugation, all atoms have sp^2 hybridization.In these compounds, the total number of π bond electrons obey the Hückel Rule (4n+2, n=1, 2, 3..), and for this reason tetrapyrrolic rings are highly stable compounds [3].

1.2. Phthalocyanines

A compound named as phthalocyanine firstly appeared in 1907, as an insoluble side product in the organic reaction of acetic acid with phthalimide performed by Braun and Tcherniac [4]. Similarly, after 20 years from the first appearance, De Diesbach and von der Weid, from Fribourg University, obtained the dark blue colored copper phthalocyanine (CuPc) in the reaction of ortho-dibromobenzene with Copper (I) cyanide in pyridine at 200°C instead of their target molecule, uncolored dinitrile compound. However, they were not able to explain the structure of their product at first step, since it was extraordinarily durable to the acids, bases and heat [5]. Another serendipitous moment happened in Scottish Dyes Ltd Company in 1928. A green-blue colored product was produced instead of phthalimide from the reaction of phthalic anhyride with ammonia [6, 7].On that occasion, the company charged the employees to analyze the compound and they thought the product was formed due to iron deformation of the reactor, and they deduced that the inspected molecule was highly stable and insoluble pigment. After Imperial Chemical Industry (ICI) bought the Scottish Dyes Ltd Company, the unidentified molecule was sent to the Prof. Jocelyn F. Trophe from Imperial College to shed on light the chemical structure of the unknown molecule and he assigned this study to Reginald P. Linstead. In this way, thanks to the collaboration of ICI and Linstead, the structure of phthalocyanines as well the synthesis of some metallophthalocyanine derivatives were elucidated [8–13].

Linstead used a variety of analysis methods such as elemental analysis, ebullioscopic method of molecular weight determination and oxidative degradation to get the exact structure of phthalocyanine which is composed of 4 iminoisoindoline rings. As a result of these studies, the similarity between phthalocyanines and porphyrin have been determined. The structural difference was identified as 4 additional benzo units and nitrogen bridges between pyrrole units. For the first time, Linstead used "phthalocyanine" term derived by using the "naphtha", mineral oil, and "cyanine", dark-blue, words for this compound [14].

1.2.1. Structure of Phthalocyanines

The phthalocyanine ring (Pc), tetrabenzotetraazaporphyrin, has a porphyrazin (Pz) like ring in which nitrogen atom exists between pyrrole rings as bridge atom. Despite the structural similarity to porphyrin, phthalocyanine is not a natural compound. It is produced synthetically in laboratories [15].

Based on Robertson's X-Ray studies with metal-free phthalocyanines, H_2Pc structure is determined in planar structure and it belongs to the D_{2h} point group of symmetry, whereas the porphyrin ring has tetragonal symmetry (D_4). So the distinction is attributed to the angles between the *meso* positioned nitrogen atoms. In Pc, the bonds composing 16-membered inner ring are shorter because bond length of the nitrogen bridges are significantly contracted. This phenomenon leads to a coordination sphere smaller than the one in porphyrin [16].

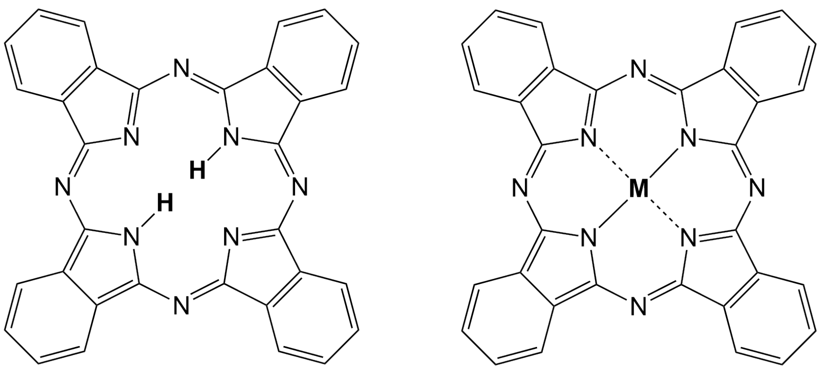

Phthalocyanine
H_2Pc

Metallophthalocyanine
MPc

Figure 1.2. The Phthalocyanine ring: non-metallated phthalocyanine (left), metal centered phthalocyanine (right).

Pc can be both metal free and metal centered as displayed in the Figure 1.2. Metallophthalocyanine forms as a result of the complexation of deprotonated Pc ring with a metal ion [17]. Phthalocyanines can be in the form of sandwich-type complexes (double decker and triple decker) as shown in the Figure 1.3, they are favored by octacoordination of large metal centers such as rare earths, actidinides and group 4 transition metals [18]. In addition to phthalocyanines with 4 isoindol unit, different types of phthalocyanines can be found in the litterature as shown in the Figure 1.4. The bor element creates subphthalocyanine (SubPc) by binding to 3 isoindol ring [19] and uranium centered phthalocyanines have 5 isoindol groups and it is called superphthalocyanines (SuperPc) [20]. Today, more than 63 metal and non metals of periodic table (e.g. Cu^{+II}, Fe^{+II}, Ni^{+II}, Zn^{+II}, Co^{+II}, Ti^{+IV}, Fe^{+III}...etc) including hydrogen can be used as central ion in phthalocyanine ring [21].

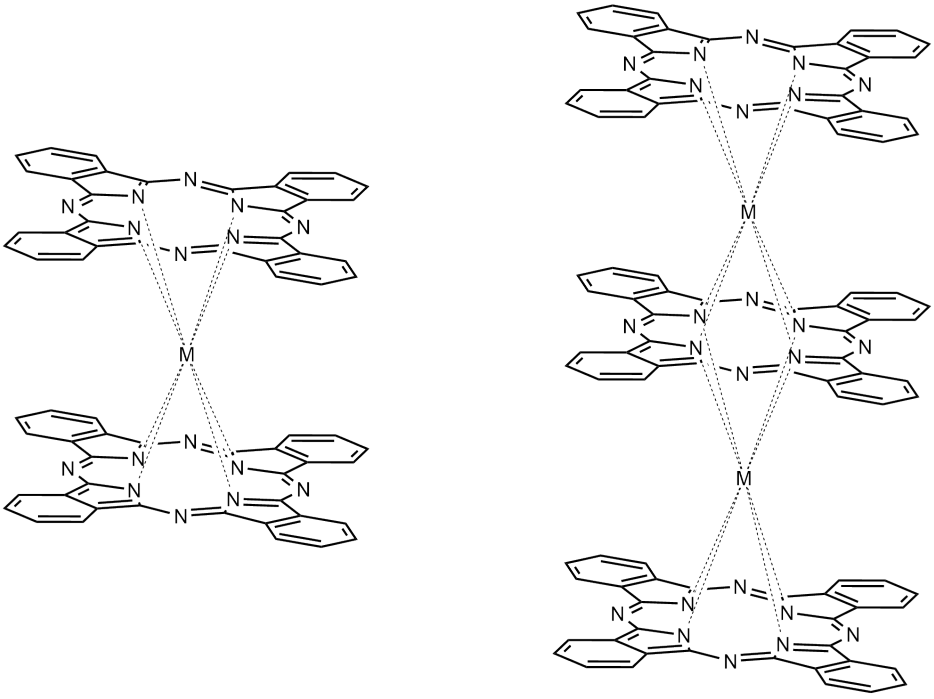

Pc_2M Pc_3M_2

Figure 1.3. Sandwich-type phthalocyanine complexes in the form of double- (left) and triple-deckers (right).

The central metal atom has an impact upon the chemical properties of phthalocyanine molecule. MPc becomes stable when the radius of the metal ion is suitable to the gap of ring. On the contrary, metals having the radii larger or smaller than the 1.35 Å are inconvenient to the center, so these metals set free from the phthalocyanine. [16]

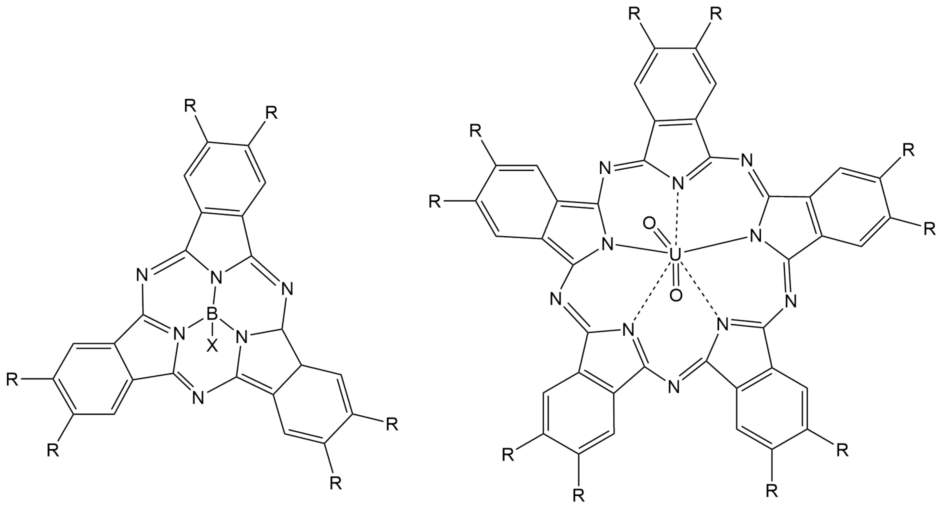

X = F, Cl, Br, OH, OR and Ph

SubPc

SuperPc

Figure 1.4. Structure of subphthalocyanine (SubPc) and superphthalocyanine (SuperPc).

Generally, the complexation of phthalocyanine ring is ended up with square planar geometry. However, when the central metal has high coordination number, the molecular geometry can be square pyramidal, tetrahedral or octahedral. Besides, by using the additional ligand such as water molecule, chlorine or pyridine, high coordination numbered complexes can also be obtained as shown in Figure 1.5.

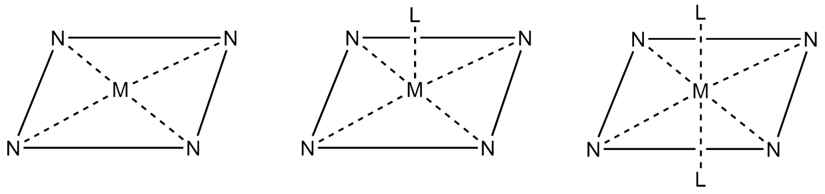

Figure 1.5. Molecular geometry of phthalocyanine molecule: square planar (left), square pyramidal (center) and octahedral (right).

The physical, chemical and electronic properties of Pcs can be tuned by adding diverse suitable substituents. The properties are enhanced when functional groups as alkyl chains, ethers, amines, thiols, halogenes and various acid groups are attached, as compared to the unsubstituted phthlaocyanine. Adding more complicated groups such crown ethers, dendrimers and ferrocenes makes the complex full-featured. To increase the variety of substitutents, ether, amine, thiol and new carbon-carbon bond can be used among the countless opportunities. There are 16 position to have a substitution reaction as displayed in Figure 1.6.

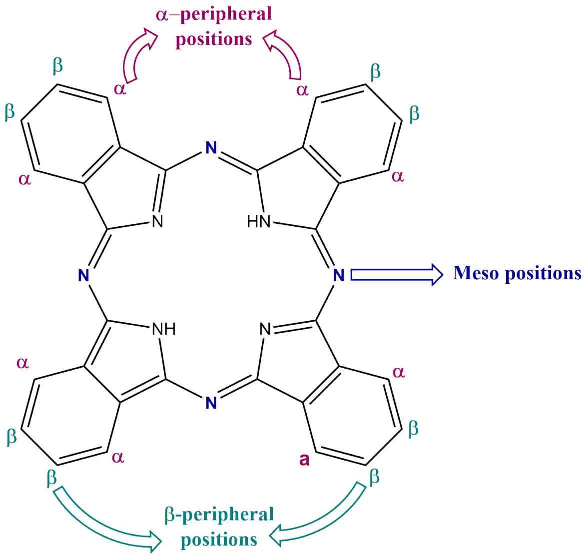

Figure 1.6. Labeling the atoms capable of the substitution and their general names.

Additionally, as a consequence of being an extended aromatic flat molecule, phthalocyanines are proned to pack with each other due to π-π stacking interactions in solutions, and therefore they generate aggregates. The aggregation severely influences the excited state properties, the excited state efficiency is reduced [22], so it also limits the application area. To overcome this issue, additional structural features such as long alkyl chains [23] are added to the α positions or the β positions are substituted with bulky groups such as large dendritic susbtituents [24–27]. This strategy allows the 18-π conjugated systems to be apart from each other, the tendency of aggregate formation is thus majorly prohibited.

1.2.2. Spectral Properties of Phthalocyanines

The chemical and electronic properties of these 16-membered rings are based on their 18-π electron system. Generally, in the absorption spectra of Pcs, around 650-720nm the intensive Q band is observed and in addition to Q band, they show less intense B band, also called Soret Band, around 300-400 nm [28]. The transition between the ground and excited states, leads to the Q band formation. The other peaks which appear in Figure 1.7 are Ligand-to-Metal Charge Transfer (LMCT) and Metal-to-Ligand Charge Transfer (MCLT), they are due to charge transfer or interactions between π-systems of dimer complexes [29].

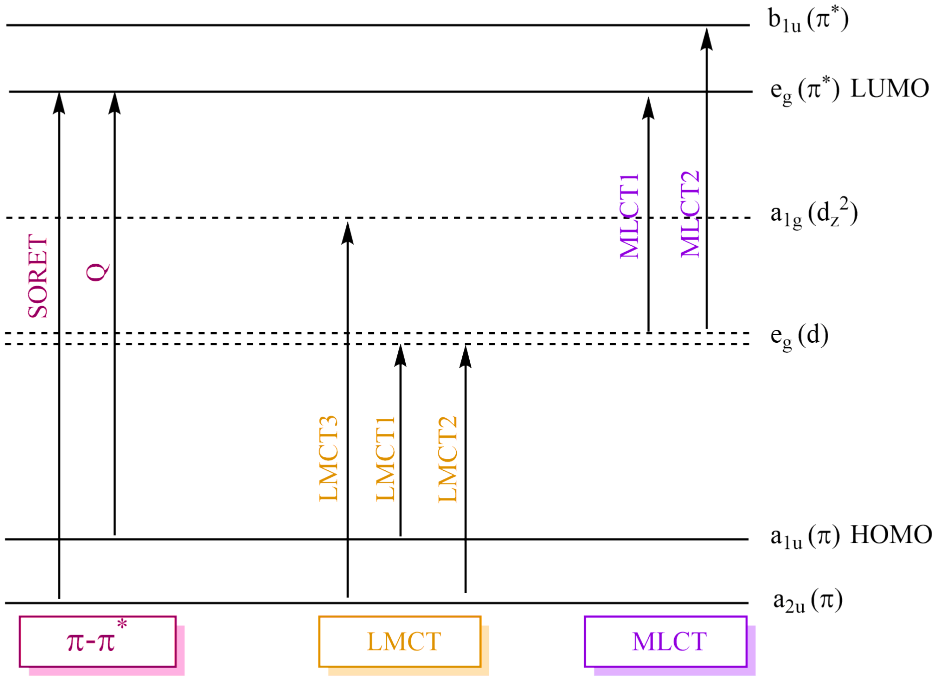

Figure 1.7. Energy levels scheme of a metallophthalocyanine, showing the origin of the various LMCT, MLCT, Q, and Soret bands.

The molecular symmetry is efficient for determining the Q band shapes (Figure 1.8). Most MPcs belong to the D_{4h} point group [30] because the contribution of metal ion stabilizes the delocalized dianion species, in a way that it helps achieving the higher symmetry. [31]. Based on study of the Gouterman *et al.* [32–35], $a_{1u}(\pi)$ is the highest occupied molecular orbital (HOMO), and the LUMO (Lowest Unoccupied Molecular Orbital) is $e_g(\pi)$ which is seen in the Figure 1.7. Strong transitions from a_{1u} and a_{2u} to e_g are attributed to Q Band and Soret band, having π-π^* character, these are common properties of metallophthalocyanines. Metal-free phthalocyanines have D_{2h} symmetry since they carry two iminic nitrogen and two nitrogen with hydrogens attached to them [31]. The split Q band is displayed in the spectrum (Figure 1.8) because of the polarization in the direction of x and y coordinates. [36].

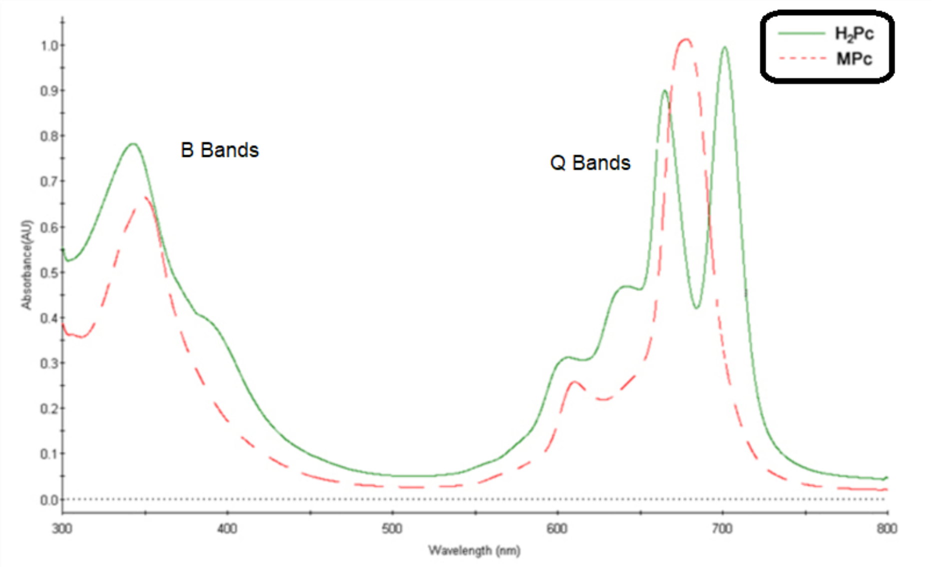

Figure 1.8. The UV absorption peaks of H_2Pcs and MPcs.

The Q band location and its intensity have an importance to specify the application area of Pc derivatives. Central metal ion, aggregation, π conjugation, molecular symmetry and substituents are the main parameters that effect the spectral properties. The aggregate arises from the high concentration levels of compound or the polar solvents usage. It may be detected in the spectrum as a shoulder of the Q band and it also causes the decrease of the band intensity [37]. In a similar manner, the ring geometry which is directly related to the aggregation formation may change the Q band intensity. In addition, tetrasubstituted phthalocyanines have tendency to form aggregate, as compared to the octasubstituted rings. Since octasubstituted ones have functional groups on both peripheral and non-peripheral positions, they cannot to be packed because of the steric hindrance.Other than that, substituents also effects the Q band location in the spectrum. A desired bathochromic shift (red shift) is observed if the functional group has electron donating character. However, the substituents on the peripheral position do not contain a function that extent the π-conjugation, they do not influence the band position [38].

In literature, there are a large number of spectral data for a great variety of complexes due to complexation with many metal ions. The oxidation state of the central metal does not considerably modify the band position. However, the central metal can play a role in connecting more than 1 ring as explained in the previous chapter (Figure 1.3), at this stage, band position may change [39]. Benihya *et al.* synthetized a triple decker phthalocyanines containing bismuth metal ion, they observed notable red shift comparing to the single phthalocyanines [40].

Phthalocyanines form aggregates in solutions as a result of being stacked on each other due to the π-π interactions. In spectra, the existance of aggregation can be monitored by hypsochromic shift. In six-coordinated MPcs, axial ligands coordinated to the metal ion prevent the aggregation formation. On the contrary, four-coordinated complexes are stacked. The addition of functional groups to peripheral and non-peripheral positions prohibits the stacking problem. In recent years, several innovative synthetic approaches have been published to get control the aggregation behavior of these complexes [41–43].

1.2.3. Application Areas

Since Pcs have intense green-blue color they have been extensively used as dyes and pigments in paint, printing, textile and paper industries. More recently, they have found broad use ranging from the industrial materials such as organic semiconductors [44], photovoltaic devices [45], gas sensors [46, 47], catalysts [48, 49] , solar cells [50, 51] to biomedical species used for bioimaging [52] and photodynamic therapy medicines [53, 54].

As mentioned in the discovery of phthalocyanines, CuPc is accidentally found as a green-blue colored product in Scottish Dyes Ltd Company in 1928 [6, 7]. Due to having large aromatic π-conjugated system, phthalocyanines, especially CuPc and its derivatives, are the best pigments (Phthalocyanine Blue) [55]. These are commercially important dyes which display color uniformity, color stability and they reveal monodispersity both in bulk state and in solution due to their prominent chemical stability [56].

Phthalocyanines are capable of coordinating to several metal ions. Depending on the properties of the metal ion, phthalocyanines can act as catalysts. Especially, Pcs containing redox-active metals catalyze efficiently several important chemical reactions such as carbon dioxide reduction to carbon monoxide [48] and oxygen reduction [49].

Pcs can have both acceptor and donor groups depending on their substituents. As a result of these features, they are also good candidates for solar cells which are devices converting sunlight to electricity. In a recent study [57], Garcia-Iglesias *et al.* synthesized ZnPc containing various functional groups with the aim of the improving the injection yield as well as the diminishing the electron transfer dynamics. The resultant Pcs have good performance by small modification of substitutent groups.

The malignant cell growth in living being is colloquially known as cancer disease which is a frequently encountered misery [58]. It is essential to cure cancer efficiently because it has a potential to expand to another part of the body. In accordance with this purpose, there have been several innovative methods, one of them being the photodynamic therapy(PDT). PDT is a promising tumor treatment in which visible light is used in conjunction with a non-toxic photosensitizer in an oxygen rich environment [59]. Pcs are effective photosensitizers in photodynamic therapy because of their intense absorption in red region of the visible light. PDT uses the photochemical interaction of three components: light at a specific wavelength (visible or near-infrared), a photosensitizer and molecular oxygen. The principles of PDT will be explained in details in next section.

In the field of medicine, the bioimaging has an importance to diagnose the disease. Traditional imaging methods (such as X-ray, magnetic resonance imaging, positron emission tomography) are not adequately sensitive and they have difficulty in specifying the lesions [60]. On the other hand, near-infrared fluorescence imaging serves high-resolution detection. Since dyes suffer less interference during cell imaging, they cause seldomly photo-damaging [61, 62]. Yokoi *et al.* published a study on the fluorescence imaging with the silicon phthalocyanine based fluorescence probe which successfully monitors the ascorbic acid in mice [63].

1.3. Photodynamic Therapy (PDT)

Photodynamic therapy is a type of a chemotherapy. It is a well-established method for the treatment of cancer, microbial infections, and skin diseases [64], in which a non-toxic photosensitizer collaborates with the oxygen and light source to damage the unhealthy cells. A sensitizer is introduced to the living body and it selectively locates the tumor by virtue of the different physiological conditions of malignants [65]. During the irradiation of the tumor with light, PS absorbs the light energy and it reacts with the molecular oxygen. As a consequence, cytotoxic singlet oxygen species are generated to cause death to the tumor cells (Figure 1.9). Unfortunately, PS is ineffective on its own and a suitable light source is not satisfactory to generate the singlet oxygen [66] because the photodynamic therapy relies on the photodynamic effect [67]. Photodynamic effect can be described as devastation of the living structures by complex action of a photosensitizer by using visible light in an oxygen rich environment.

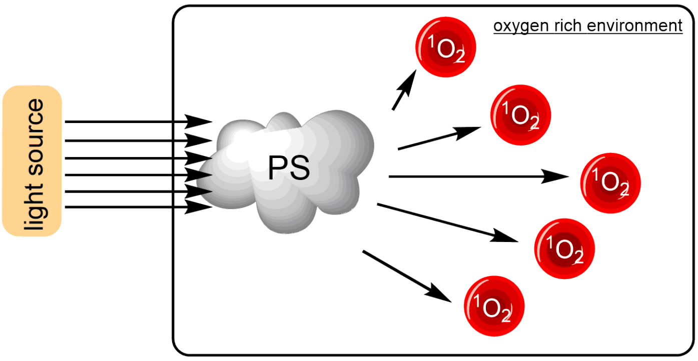

Figure 1.9. Representation of the singlet oxygen generation.

A PS or a photosensitizing agent (drug) is excited by absorbing light and it stores energy. During its return to the ground state, it may follow several pathways as indicated in the Figure 1.10. One of them is the production of heat which is also known as internal conversion (IC). Another return path is the fluorescence emission in which a light beam, having the energy difference between the excited and ground states, is emitted. Moreover, an excited PS may relax its energy by changing the spin of the excited electron and undergo the intersystem crossing. As a consequence, excited triplet state is generated. Yet, based on the photophysical rules, electrons in singlet state cannot pass to the triplet state. It is defined as spin-forbidden transition and the spin change of the unpaired electron is closely related to the degree of the spin-orbit coupling term (SOC) of the system [68].

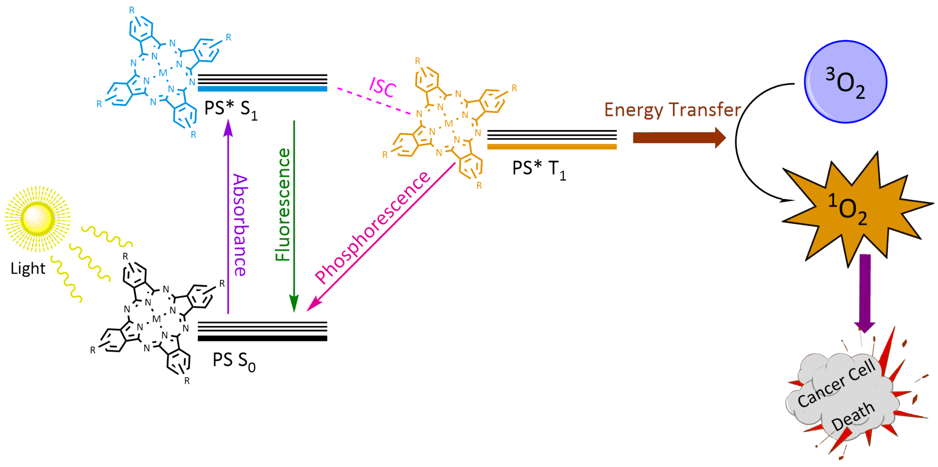

Figure 1.10. Jablonski Diagram of the mechanism of photodynamic therapy.

As well as returning to the ground state involves the prohibited triplet-singlet transition, the excited PS has triplet lifetime (at microseconds) which is adequate to promote oxygen. On the other hand, the multiplicity of the molecular oxygen ($^3O_2$) is triplet. At this point, the energy transfer actively occurs from the triplet excited state of the electron rich PS compound to the triplet ground state of the molecular oxygen, because of the spin-allowed transition. Similarly, the excited oxygen molecule ($^1O_2$) has a lifetime around microseconds at singlet state due to spin-forbidden transition and this time interval is sufficient to destroy the unhealthy tissues [69–71].

An excited triplet state reacts with oxygen in 2 different ways: Type I and II mechanisms (Table 1.1). Type I produces free radicals by a hydrogen abstraction reaction or electron transfer from the excited sensitizer to a substrate. These radicals interact with the oxygen and reactive oxygen species (ROS) is generated [72]. The other mechanism, Type II, is much simpler mechanism than Type I and most of the PS used in this treatment are credited to function through the energy transfer process because the singlet oxygen is the main reason of the oxidative cellular damage resulting in necrosis or apoptosis of the biological tissue [73, 74]. The efficiency of the treatment is mainly dependent on the oxygen concentration in environment, light sources and its wavelength, and photosensitizer. During the treatment, the surrounding molecular oxygen concentration is continuously consumed due to turning into singlet oxygen species.

Table 1.1. Reactions during photodynamic action [75].

Excitation	$^1PS + hv \rightarrow {}^1PS^* \rightarrow {}^3PS^*$
Photoprocess	Reactants → Products
Type I	$^3PS^*+{}^1PS \rightarrow {}^3PS^{-\bullet}+O_2$
	$^3PS^*+D \rightarrow PS^{-\bullet}+D^+$
	$^3PS^{-\bullet}+O_2 \rightarrow {}^1PS+O_2^{-\bullet}$
	$^3PS^*+O_2 \rightarrow {}^3PS^{+\bullet}+O_2^{-\bullet}$
	$^2O_2^*+2H^+ \rightarrow O_2+H_2O_2$
Type II	$^3PS^*+{}^3O_2 \rightarrow {}^1PS^*+{}^1O_2$

1.3.1. Photosensitizers in PDT

The π-conjugated system of the PS influences the singlet oxygen quantum yields (Φ_Δ) because it is strongly dependent on the intersystem crossing rate and the energy separation between singlet and triplet excited states [76]. Most of molecules having UV-visible absorbance are able to generate singlet oxygen, but they meet the following criteria to be used as appropriate photosensitizers in the treatement. They commonly must have [65, 72]:

- Intense absorption in near-IR region of the visible spectrum with high extinction coefficient,
- Ability to generate the singlet oxygen with high quantum yield,
- Reproducibility and accesible synthetic route,
- Chemical and thermal stability,
- Solubility in the biological environment,
- Effective accumulation in malignant tissue,

- Low aggregation tendency in solution,
- Excretion after treatement.

A literature survey indicates that several strategies have been performed to develop novel PSs that fulfill these requirements [59, 65, 72, 76–78]. Moreover, the drug needs to be easily carried into the body and that is the reason why photosensitizer should be not only watersoluble for biocompatibility but also lipophilic for diffusion through the cell membrane. [65, 79–81]. PSs are classified as generations. First generation photosensitizers are derivatives of hematoporphyrin compound. In this class, the first clinically approved and commercially available photosensitizers are Photofrin® and Photogem® [65, 82, 83]. Even if they are entitled to be used in experimental clinical researches, the first generation PSs are suffered from lack of selectivity, low absorption in red region of visible spectrum and skin phototoxicity [65, 78]. The second generation PSs are aimed to overcome these problems. Generally, they have absorbance in long wavelength regions with high molar absorption coefficient, rapid and selective detection of cancer cells and easy elimination from the body [59, 72]. Porphyrins, phthalocyanines and related tetrapyrrole compounds belong to this class. Since porphyrins are present in natural systems, thus these generation attracts a great deal of attention for biological singlet oxygen production [72]. Phthalocyanines, which have similar skeletons as porphyrins, participate in PDT as photosensitizer and they have outstanding features such as having intense molar absorptivity in IR region and longer triplet lifetime and being photostable. Phthalocyanines meet most of the factors stated above, for that reason, these compounds are nominated as good candidates for the treatment. On the other hand, their tendency of formation of aggregates in solutions is a serious problem because in such cases, the efficiency of phthalocyanine as PS drug is low.

1.4. Aim of the Study

In this thesis, the main purpose is to determine the suitability of phthalocyanines to be used as photosensitizers in photodynamic therapy by clarifying their photophysical properties. Pentafluorobenzyloxy substituted phthalocyanines with three different centers (H_2, Zn and Ni) [84] and their unsubstituted versions are chosen (Figure 1.11).

Since the photosensitizer used in this treatment has to meet the photophysical criteria, there may be predominant reasons such as metal effect, substitution effect which may improve the photosensitizer's efficiency. In accordance with this purpose, their excited state characteristics have been studied by using Time-Dependent Density Functional Theory.

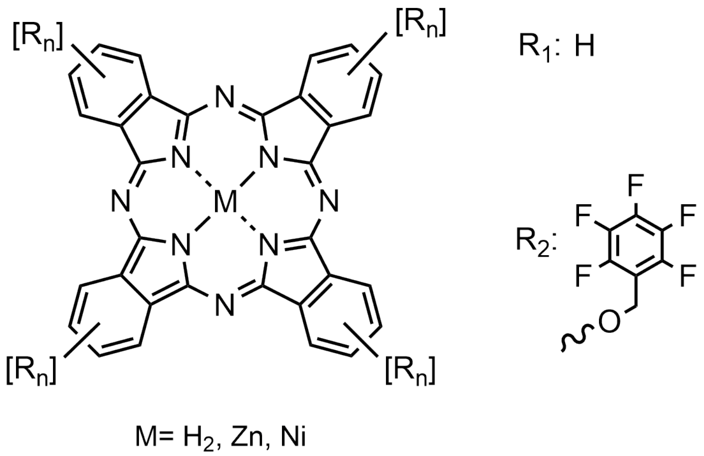

Figure 1.11. Unsubstituted (R_1) and pentafluorobenzyloxy- substituted (R_2) metallophthalocyanines and their free base analogues.

2. METHODOLOGY

In quantum chemistry, the main task is to solve Schrödinger equation since the wavefunction contains the information about the particle. As an example, according to the Heisenberg Uncertainity Principle [85] the determination of the exact position and the momentum of a particle cannot be possible at the same time. However, the probability of the positions of that particle can be calculated by squaring the wavefunction which is found by solving the Schrödinger's equation:

$$H\psi = E\psi \tag{2.1}$$

in which H represents the Hamiltonian Operator, and it gives the total energy (E) of the system as an eigenvalue and ψ corresponds the wavefunction. H operator is composed of kinetic and potential energy terms of the nuclei and the electrons:

$$H = -\sum_i \frac{\hbar^2}{2m_e}\nabla_i^2 - \sum_k \frac{\hbar^2}{2m_k}\nabla_k^2 - \sum_i \sum_k \frac{e^2 Z_k}{r_{ik}} + \sum_{i<j} \frac{e^2}{r_{ij}} + \sum_{k<l} \frac{e^2 Z_k Z_l}{r_{kl}} \tag{2.2}$$

where electrons are represented as i and j, nuclei are symbolized as k and l, $\mathrm{m_k}$ and $\mathrm{m_e}$ are the masses of nuclei and electrons, respectively, $\hbar$ is the "h/2π" where h is the Plank's constant,r, e is the electron charge, Z is atomic number and r is the distance between the particles and ∇^2 is the Laplacian operator. In the Equation 2.2, all five components express the energy of the system. The first two terms give the kinetic energy value of electrons and nuclei, respectively. The other terms imply the potential energies which are resulted from Coulomb interactions of nucleus-electron, electron-electron and nucleus-nucleus.

The Schrödinger equation is accurate for small systems such as the hydrogen atom and the hydrogen-like ions, but it cannot give an exact solution for many-particle systems due to the associative motions of particles. Since the nuclei are much heavier than electrons, they are appeared as stationary charged point, compared to the electrons. So their kinetic energy terms will be zero. Born-Oppenheimer approximation [86] proposes to treat the electronic and nuclear motions separately, to eliminate the nucleus-electron attraction term and to take nuclear-nuclear repulsion term constant. With respect to this approach, Hamiltonian operator becomes:

$$H_{el} = E_k^{kin} + U_{ki} + U_{ij} \tag{2.3}$$

where U_{ki} and U_{ij} are the potential energy of nucleus-nucleus and electron-electron interactions, respectively. After applying this approximation to the Schrödinger equation, then it becomes:

$$(H_{el} + V_{nn})\psi_{el} = E_{el}\psi_{el} \tag{2.4}$$

where V_{nn} is the nucleus-nucleus repulsion energy constant, and the E_{el} as an eigenvalue, is the electronic energy.

The refined Schrödinger equation (Equation 2.4) can be used for all other systems by using variational principle. By multiplying both sides of the Equation 2.1 with ψ, it becomes:

$$\psi H \psi = \psi E \psi \tag{2.5}$$

For many electron systems, integration of both sides in a volume ($d\tau$) yields:

$$\omega = \frac{\int \psi H \psi d\tau}{\int \psi^2 d\tau} \tag{2.6}$$

This theorem states that calculated energy value (ω) can only be greater than or equal to the ground-state energy E_0, ($\omega \geq E_0$). It gives an approximate solutions of Schrödinger equation. The methodologies that used in this study is mainly based on Density functional theory which is a variational method.The theory of it will be explained in detail, in the next section.

2.1. Density Functional Theory

A widely used quantum chemistry approach, Density Functional Theory (DFT) [87], was suggested in 1964 by Hohenberg and Kohn [88, 89]. Hohenberg-Kohn Existance Theorems [90] are the basis of DFT. It allows the calculation of the electronic structure of molecules. With regard to theorem, the wavefunction can be determined if the ground state density of the system is known. They proof an association between the external potential (V_{ext}(r)) and the electron density (ρ(r)) that, V_{ext}(r) is a function of ρ(r). The electron density is defined as seen in Equation 2.7 in which r_i represents the coordinates of the electrons.

$$\rho(r) : N \int ... \int |\Psi(r_1, r_2, ...r_n)|^2 dr_1 dr_2 ... dr_n \tag{2.7}$$

Their second theorem states that by using variational principle, the ground state enery can be obtained because the ground state density is the density that minimizes the total energy [90]. The ground state electronic energy as a function of the electron density is :

$$E[\rho(r)] = \int V(r)\rho(r)dr + T[\rho(r)] + V_{ee}[\rho(r)] \tag{2.8}$$

The Equation 2.8 can be rewritten by using the theory developped by Kohn and Sham [91]. The electronic energy equation becomes:

$$E[\rho(r)] = \int V(r)\rho(r)d(r) + T_{ni}[\rho(r)] + J[\rho(r)] + E_{XC}[\rho(r)] \tag{2.9}$$

The terms are the coulomb energy (J[ρ]), the kinetic energy of non-interacting electrons ($\mathrm{T_{ni}}[\rho]$) and the exchange-correlation energy functional ($\mathrm{E_{XC}}[\rho]$). The Coulomb energy of electron-electron interactions term does not take into account the correlation between the motions of electrons. It can be represented as:

$$J[\rho(r)] = -\sum_{A=1}^{M} \int \frac{Z_A}{\mid r - R_A \mid}\rho(r)dr + \int \frac{\rho(r_1)\rho(r_2)}{\mid r_1 - r_2 \mid} dr_1 dr_2 \tag{2.10}$$

where M is the total number of nuclei. The kinetic energy term describes the measure of the freedom for non-interacting electrons, It can be expressed as follows:

$$T_{ni}[\rho(r)] = \sum_{i=1}^{N} \int \psi_i(r) - \frac{\nabla^2}{2}\psi_i(r)dr \tag{2.11}$$

in which N is the total number of electrons. The latter term of the Equation 2.9, being the exchange-correlation energy functional, it is designated as the sum of an exchange functional ($\mathrm{E_X}[\rho]$) and a correlation functional ($\mathrm{E_C}[\rho]$), although it correlates with the kinetic energy term arising from the kinetic energy difference between the interacting and non-interacting electron systems [92]. The exchange correlation energy is:

$$E_{XC}[\rho(r)] = \int \rho(r)\epsilon_{XC}(\rho(r))dr \tag{2.12}$$

The derivative of Equation 2.12 with respect to the electron density, the following equation is obtained:

$$V_{XC}[\rho(r)] = \rho(r)\frac{d\epsilon_{XC}(\rho(r))}{d\rho(r)} + \epsilon_{XC}(\rho(r)) \tag{2.13}$$

In Kohn-Sham density functional theory, the independent orbitals ψ_i, also known as Kohn-Sham orbitals are established by solving the Kohn-Sham equations.

$$h_{KS}\psi_i = \varepsilon_i\psi_i \tag{2.14}$$

in which the h_{KS} is the hamiltonian operator of Kohn-Sham, it is defined as:

$$h_{KS} = -\frac{\nabla^2}{2} - \sum_{A=1}^{N} \frac{Z_A}{\mid r - R_A \mid} + \int \frac{\rho(r_1)\rho(r_2)}{\mid r_1 - r_2 dr_1 dr_2} V_{XC}[\rho(r)] \tag{2.15}$$

where V$_{XC}[\rho(r)]$ is the exchange correlation potential. It is related with the exchange-correlation energy as seen in the Equation 2.13. If the exact form of the exchange-correlation functional is known, the Kohn-Sham orbitals give the exact density by the following equation:

$$\rho(r) = \sum_{i=1}^{N} |\psi_i|^2 \tag{2.16}$$

However, the exact form of exchange-correlation functional is not known and functionals represent the different approximations to this exchange-correlation functional.

2.2. Functionals

As DFT was developed, different approximations have been invented with the aim of determining the exact form of the exchange-correlation functional. The first approximation,Local Density Approximation (LDA), is the base of the exchange-correlation functionals. This approach gives the energy of a uniform electron gas, it treats the electron density of a given system as equal in each site and the positive charge accompanies to make the system neutral. The energy expression is

$$E[\rho] = T_{ni}[\rho] + \int \rho(r)v(r)dr + J[\rho] + E_{xc}[\rho] + E_b \tag{2.17}$$

where E$_b$ is the electrostatic energy of the positivity. Since electron density and positive charge density are equal to each other, the Equation 2.17 can be reduced to:

$$E[\rho] = T_{ni}[\rho] + E_{xc}[\rho] \tag{2.18}$$

and the E_{xc} term can be divided into two parts: an exchange functional and a correlation functional. The Equation can be rewritten by replacing the E_{xc} term with these functionals:

$$E[\rho] = T_{ni}[\rho] + E_x[\rho] + E_c[\rho] \tag{2.19}$$

The kinetic energy functional is

$$T_{ni}[\rho] = C_F \int \rho(r)^{5/3} dr \tag{2.20}$$

with C_F constant equal to 2.8712. The exchange functional can be found by using the following equation:

$$E_x[\rho] = -C_x \int \rho(r)^{4/3} dr \tag{2.21}$$

with C_x constant equal to 0.7386. The correlation energy term, $E_c[\rho]$, for uniformly distributed electron gas is obtained from the parametrization of the results of a set of quantum Monte Carlo calculations. However, LDA is not suitable to determine the exact form of the exchange-correlation functional. The electron density cannot be uniformly distributed since the electron densities vary in a molecule .

Generalized gradient approximaton (GGA) [93] methods consider the inhomogenous nature of electron density by postulating the exchange and correlation energies dependent not only the density, but also on its gradient. The energy expression is

$$E_{XC}^{GGA}[n] = \int n(r)\epsilon_{XC}(n(r), |\nabla n(r)|) dr \tag{2.22}$$

An alternative approach is the hybrid density functional methods which is a combination of the GGA method with a percentage of Hartree-Fock (HF) exchange. These functionals add the exact exchange calculated through HF functional to DFT exchange and correlation. The most well-known one is B3LYP [88, 94] . It has the form of a mixture of LDA and GGA functionals as illustrated:

$$E_{XC}^{B3LYP} = (1-a)E_{X}^{LSDA} + aE_{X}^{HF} + b\Delta E_{X}^{B} + (1-c)E_{C}^{LSDA} + cE_{C}^{LYP} \tag{2.23}$$

where the empirical coefficients are determined to be 0.20, 0.72 and 0.81, respectively [95].

Another approch is the long-range corrected (LC) hybrid density functionals employing 100% HF exchange for long-range electron-electron interactions. A long range corrected hybrid of a density functional approximation (LCDFA) is described as:

$$E_{XC}^{LCDFA} = E_{X}^{SR-DFA}(\omega) + E_{X}^{LR-HF}(\omega) + E_{C}^{DFA} \tag{2.24}$$

The long range correction improves such features as long-chain polarizability, charge-transfer excitations, optical properties and dissociation of two-centered three electrons bonds [96]. ωB97XD [97] is one of the (LC) hybrid density functionals, having a small fraction around 22% for short-range exact exchange.

2.3. Basis Sets

John C. Slatter first described the orbitals within a system as a set of functions, called basis set [98]. They are necessary to be identified in order to solve the Schrödinger Equation. Basis functions are usually expanded as a linear combination of atomic orbitals (LCAO) with coefficients.

Basis sets are composed of mainly 2 classes: Slater-type orbitals (STOs) and Gaussian-type orbitals (GTOs). Even though STO is accurate to give the solution to Schrödinger equation for hydrogen atoms, their computational cost is high. On the other hand, GTOs are preferable over STOs because the increasing the number of integrals brings about the increase of the computational time. GTOs developed by S. Francis Boys [99], are widely utilized basis sets in DFT studies. They are the approximated analogues of STOs.

Split-valence basis sets developped by Pople *et al.*, treat differently the core and valence orbitals. Only one basis functional is applied to each core atomic orbitals, and a larger basis is used for the valence atomic orbitals. 3-21G,6-21G, 6-31G*, 6-311G** and 6-31++G** are the mostly known ones. The former number is the primitives for inner shell orbitals, and the numbers after the hyphen denote the number of primitives used for the valence orbitals: Two The modification of the basis sets can be possible with the addition of two functions to get better approximation to the exact electronic energy: polarization and diffuse functions. Polarization functions add higher angular momentum orbital to all heavy atoms symbolized by one asteriks * or (d). In order to include the polarization of light atoms such as hydrogen and helium, two asteriks are used. Additionally, diffuse functions are represented as "+", they allow orbitals to occupy larger spaces. One plus sign indicates diffuse functions are only added for the heavy atoms and "++" denotes diffuse functions are added to hydrogen atoms.

2.4. Polarizable Continuum Model

In quantum chemical calculations, solvation models provide a solvent environment in order to obtain more realistic results for the system. They may be either taken implicitly and/or explicitly. In explicit solvation models, the solvent molecules as a discrete number, are explicitly added into the model. The implicit solvent models describe a solvent continuum. They are the most efficient way to include condensed-phase effects into the quantum chemical calculations. The implicit solvent model is also called continuum solvation model, includes different physical effects which contribute to overall solvation process. The total solvation free energy is expressed as

$$\Delta G_{solvation} = \Delta G_{cavity} + \Delta G_{dispersion} + \Delta G_{electrostatic} + \Delta G_{repulsion} \tag{2.25}$$

In this equation, ΔG_{cavity} is the energy of adding solute in the system environment. $\Delta \text{G}_{dispersion}$ is the energy of interactions between solvent and solute, it adds the stabilization to solvation free energy. The electrostatic interactions energy of solute-solvent is $\Delta \text{G}_{electrostatic}$ and $\Delta \text{G}_{repulsion}$ is the exchange solute-solvent interactions which are not included in the ΔG_{cavity}. All terms are calculated by use of a defined cavity through interlocking van der Waals spheres centered at atomic positions.

Polarizable Continuum Model (PCM) developped by Tomasi *et al.* [100], is one of the polarizable continuum solvation models. In PCM, a cavity is formed by a set of spheres centered on atoms, having radii identified by the van der Waals radii of the atoms multiplied by a constant factor, the solute is placed in this cavity. Then, The polarization charges are embedded into small domains which are formed by the subdivision of the cavity. PCM method assumes that the solvent has a single specific dielectric constant and the charge distribution of the solute induces a polarization.It has mainly 3 different approaches called Dielectric PCM (D-PCM), Conductor-like PCM (C-PCM) and Integral Equation Formalism of PCM (IEF-PCM). The former one is the first formulation of PCM. The second one provides a solvation act as a surrounding medium which is modeled as a conductor, instead of a dielectriç. The latter one is an implementation whereby the PCM equations are reformed.

2.5. Time Dependent Density Functional Theory

Time Dependent Density Functional Theory (TD-DFT) is a computational tool that provides the calculation of electronic excited properties of systems. As the Hohenberg Kohn Theorem is the base of DFT, TD-DFT is based on the Runge-Gross Theorem [101]. It is namely a time-dependent analogue of Hohenberg-Kohn Theorem. According to their approach, the hamiltonian operator can be expressed:

$$\widehat{H} = \widehat{T}(r) + \widehat{W}(r) + \widehat{V}_{ext}(r,t) \tag{2.26}$$

where the $\widehat{T}(r)$ represents the kinetic energy of electrons, $\widehat{W}(r)$ describes the Coulomb interaction between the electrons and the latter term, $\widehat{V}_{ext}(r,t)$, defines the time-dependent potential effect on electrons. The excited state energy mainly depends on the external potential, and for that reason, the determination of the effects of the potential on the system is necessary in order to calculate the excited state properties.

The Hohenberg-Kohn Theorem is applied a variational principle as shown

$$A = \int_{t_0}^{t_1} \langle \Psi(t) | i \frac{\partial}{\partial_t} - \widehat{H} | \Psi(t) \rangle dt \tag{2.27}$$

and the wavefunction is determined up to a time-dependent constant:

$$\Psi(r_1, ..., r_N, t) = \Psi[\rho](t) e^{-ia(t)} \tag{2.28}$$

The phase factor adds a constant to the action in Equation 2.28:

$$A[\rho] = \int_{t_0}^{t_1} \langle \Psi(t) | i \frac{\partial}{\partial_t} - \widehat{H}(t) | \tilde{\Psi}[\rho](t) \rangle dt + a(t_1) - a(t_0) = A[\rho] + const. \tag{2.29}$$

And A$[\rho]$ can be written as:

$$A[\rho] = B[\rho] - \int dr \int_{t_0}^{t_1} (r, t) \rho(r, t) dtv \tag{2.30}$$

where B$[\rho]$ represents the independent of the external potential. Assuming that an independent system has the property described as illustrated:

$$\rho(r, t) = \sum_i f_i |\Psi(r, t)|^2 \tag{2.31}$$

The B$[\rho]$ term can be rewritten as

$$B[\rho] = \Sigma_i f_i \int_{t_0}^{t_1} \langle \Psi_i(t) | i \tfrac{\partial}{\partial_t} - \tfrac{1}{2} \nabla_i^2 | \psi_i(t) \rangle dtv - \tfrac{1}{2} \int_{t_0}^{t_1} dt \iint dr_1 dr_2 \tfrac{\rho(r_1,t)\rho(r_1,t)}{|r_1 - r_2|} - A_{XC}[\rho] \tag{2.32}$$

In this equation, $\mathrm{A_{XC}}[\rho]$ is the exchange and correlation action functional. Applying the variational principle to Equation 2.30 with constraint results:

$$\rho(r, t) = \sum_i f_i |\Psi_i(r, t)|^2 = \sum_i^N |\Psi_i(r, t)|^2 \tag{2.33}$$

Time-dependent Kohn-Sham equation is obtained:

$$[-\frac{1}{2}\nabla^2 + v_{eff}(r,t)]\Psi_i(r,t) = i\frac{\partial}{\partial_t}\Psi_i(r,t) \tag{2.34}$$

$$v_{eff}(r,t) = v_H(r,t) + v_{xc}(r,t) + v_{ext}(r,t) \tag{2.35}$$

where the unknown is the time-dependent exchange potential. In equation 2.34, all exchange and correlation effects are collected:

$$v_{xc}(r,t) = \frac{\delta A_{xc}[\rho]}{\delta\rho(r,t)} \tag{2.36}$$

Time dependent density functional theory equations are exact with no approximations made. However, to determine the unknown term, the exchange-correlation functional, adiabatic approximation (AA) is introduced:

$$v_{xc}[\rho](r,t) = \frac{\delta A_{xc}[\rho]}{\delta\rho(r,t)} \approx \frac{\delta E_{xc}[\rho]}{\delta\rho(r)}|_{\rho=\rho(r,t)} \tag{2.37}$$

If the electron densities change, the exchange and correlation potential change instantaneously.

2.6. Wigner Distribution Function

The Wigner distribution function (WDF) was first propounded by E. Wigner as a quantum corrections to classical mechanics [102]. The Wigner quasi-probability distribution, also known as Wigner-Ville Distribution (WVD), was proposed with the aim of the associating the wavefunction with the probability distribution in phase space. The combined distribution of the particle coordinates and momentum are described in terms of wavefunction, Ψ.

The Wigner distribution $W(x,p)$ can be generated by using either the coordinate-space or momentum-space wavefunction. The Wigner transform by using the coordinate-space wavefunction, can be written for one-dimensional system :

$$W(x,p) = \frac{1}{2\pi}\int_{-\infty}^{\infty} \psi^*(x+\frac{s}{2})\psi(x-\frac{s}{2})e^{ips}ds \tag{2.38}$$

where ψ denotes the wavefunction, x is the position and p is the momentum of any conjugate pair. The $\psi^*(x+\frac{s}{2})$ and $\psi(x-\frac{s}{2})$ terms can be rewritten as illustrated in following equations,

$$\psi^*(x+\frac{s}{2}) = \langle\psi|x+\frac{s}{2}\rangle \tag{2.39}$$

$$\psi(x-\frac{s}{2}) = \langle x-\frac{s}{2}|\psi\rangle \tag{2.40}$$

Assigning $1/2\pi$ to the third term of the Equation 2.38, e^{ips}, and momentum eigenfunction in coordinate space and its complex conjugate, the third term becomes

$$\frac{1}{2\pi}e^{ips} = \frac{1}{\sqrt{2\pi}}e^{ip(x+\frac{s}{2})}\frac{1}{\sqrt{2\pi}}e^{-ip(x-\frac{s}{2})} \tag{2.41}$$

this equation can be rewritten as

$$\frac{1}{\sqrt{2\pi}}e^{ip(x+\frac{s}{2})}\frac{1}{\sqrt{2\pi}}e^{-ip(x-\frac{s}{2})} = \langle x+\frac{s}{2}|p\rangle\langle p|x-\frac{s}{2}\rangle \tag{2.42}$$

Substituting Equations 2.39, 2.40 and 2.42 into the Equation 2.38, it becomes,

$$W(x,p) = \int_{-\infty}^{\infty} \langle\psi|x+\frac{s}{2}\rangle\langle x+\frac{s}{2}|p\rangle\langle p|x-\frac{s}{2}\rangle\langle x-\frac{s}{2}|\psi\rangle ds \tag{2.43}$$

The consecutive four brackets are described respectively. The first is the amplitude of a particle in the state ψ having the position $(x-\frac{s}{2})$; the second one is the amplitude that a particle having the position $(x-\frac{s}{2})$ with momentum p; third term is the amplitude of a particle having the momentum p with the position $(x + \frac{s}{2})$; the latter one is the amplitude that a particle with position $(x + \frac{s}{2})$ in ψ state. The integration over s creates a superposition of all possible quantum trajectories of the state ψ, which interfere constructively and destructively, providing a quasi-probability distribution in phase space (Figure 2.1) [103].

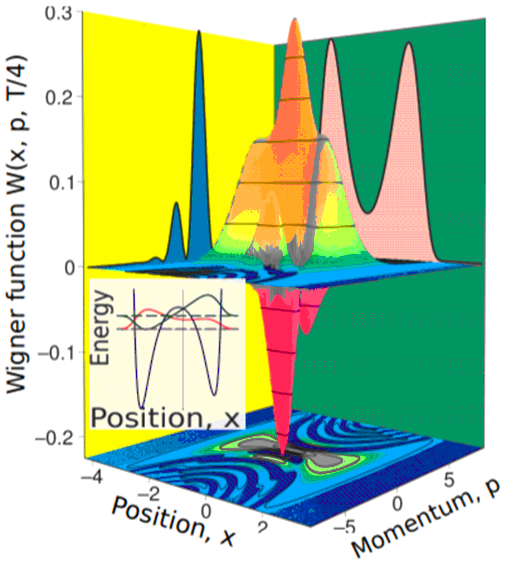

Figure 2.1. Wigner function graphic $W(x, p)$, showing momentum and position probability distribution

In a recent study, Zobel *et al.* compared the excited state properties calculated by a single ground state geometry and geometries generated by using vibrational sampling technique based on WDF from ground state geometry. This comparative study indicates that the the appearance of a shoulder on absorption band can not be explained by the single ground state geometry, however, the experimental spectra are in good agreement with the excited state properties performed by the generated geometries [104].

2.7. ϕ_s Index

ϕ_s index is a descriptor of light-induced electronic charge density variation. It is a very straightforward way to describe charge transport occuring upon light-absorption. ϕ_s index is obtained by the way of density matrices analysis. Difference of density matrix Δ is obtained by the diffraction between the ground state matrix P_0 and excited state density matrix P_X, as shown:

$$\Delta = P_X - P_0 \Rightarrow \sum_{k=1}^{K} (\Delta S)_{kk} = 0 \tag{2.44}$$

where ΔS term can be negligible, since the system does not gain or lost electrons. After a unitary similarity transformation is performed on Δ, the diagonal matrix δ is obtained:

$$\exists U | \delta = U^{\dagger} \Delta U; \quad (\delta)_{ij} = 0 \quad \forall i \neq j \tag{2.45}$$

Afterwards, the diagonal matrix is divided into two arrays according to their signs. The resultant diagonal matrices are backtransformed to obtain the Detachment Γ and Attachment Λ density matrices. [105] The detachment is the deficiency of electron density that stems from light absorption. Attachment represents the increase in electron density at excited state. They are expressed in the space of K atomic orbitals. Because of the fact that no electron is lost during the vertical excitation, one can see that:

$$\sum_{\mu=1}^{K} (\Gamma S)_{\mu\mu} = \sum_{\mu=1}^{K} (\Lambda S)_{\mu\mu} \tag{2.46}$$

Besides, related detachment/attachment densities can be described in 3D space. Spatial distribution of the electronic density removed (detachment) from the ground state and reorganized (attachment) in the excited state during transition identified by equations below, in which detached/attached charge can be expressed:

$$\theta = \int_R d\xi_1 \int_R d\xi_2 \int_R d\xi_3 \varrho_\tau(\xi_1 \xi_2 \xi_3) \equiv \int_{R^3} d^3\xi_{\varrho\tau}(\xi) \tag{2.47}$$

$$\tau \equiv \Gamma, \Lambda \tag{2.48}$$

And, the dimensionless ϕ_s index as the overlap between the attachment and detachment densities can be written as:

$$\phi_S = \theta^{-1} \int_{R^3} d^3\xi \sqrt{\varrho_\Gamma(\xi)\varrho_\Lambda(\xi)} \tag{2.49}$$

The ϕ_S index, dependent on the charge-transfer character of the electronic transition, can take values ranging from 0 to 1.In the conditions that ϕ_S index is equal to 0, there is no overlap between detachment and attachment densities. On the contrary, if the descriptor is equal to 1 in an extreme case, which means that no electronic density fluctuation exist between ground and excited states (Figure 2.2).

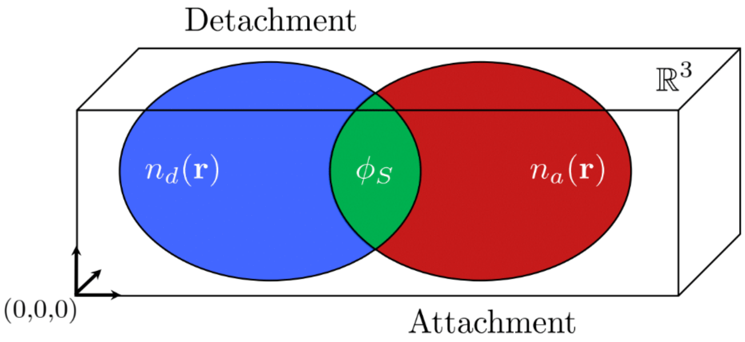

Figure 2.2. Graphical description of ϕ_S index quantum descriptor as the overlap between density matrices.

2.8. Spin-Orbit Interaction

The spin-orbit interaction, also called as spin-orbit coupling, is the relativistic interaction between the spin of the particle and its motion inside a potential. Electrons act as small magnets due to their spin . Additionaly, since they orbit around the nucleus, their orbital motion leads them to be acting as a magnet. These two magnetic moments may interact with each other and this coupling is defined as spin-orbit coupling (SOC).

Each electron has two angular momenta called orbital angular momentum ($\overrightarrow{l}$) and spin angular momentum ($\overrightarrow{s}$) as shown in the Figure 2.3.

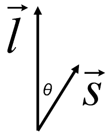

Figure 2.3. Orbital angular momentum vector and spin angular momentum vector.

The total momentum ($\overrightarrow{j}$) is found by their vectoral addition:

$$\overrightarrow{j} = \overrightarrow{l} + \overrightarrow{s} \tag{2.50}$$

so the total momentum quantum number is either a full or half integrer in the range of j$_{min}$ and j$_{max}$.

$$j_{max} = l + s = l + \frac{1}{2} \tag{2.51}$$

$$j_{min} = |l - s| = |l - \frac{1}{2}| \tag{2.52}$$

where the total momentum cannot be equal to a negative value.

In classical mechanics, an electron moving in an orbit with angular momentum L has mass M and charge would have a magnetic moment

$$\mu = -\frac{e}{2M}L \tag{2.53}$$

suggesting that in the quantum case;

$$\hat{\mu} = -\frac{e}{2M}\widehat{L}, \hat{\mu}_z = -\frac{1}{2M}\widehat{L}_z \tag{2.54}$$

the eigenvalues of $\hat{\mu_z}$ are found as

$$\hat{\mu_z} = -\frac{e\hbar}{2M}m_l \equiv -\mu_B m_l \tag{2.55}$$

in which the μ_B is known as *Bohr magneton.*

The magnetic moment is also related with the intrinsic spin of the electron:

$$\hat{\mu}_z = -\frac{g_s e}{2M}\widehat{S}_z \tag{2.56}$$

where g_s is the constant that cannot be determined by using classical arguments but it is predicted to be 2 by the relativistic quantum theory.

The interaction between these two magnetic moments of electron introduces an extra term into the Hamiltonian of the form

$$\widehat{H}_{S-O} = f(r)\widehat{L}\widehat{S} \tag{2.57}$$

and f(r) can be defined as

$$f(r) = \frac{1}{2M^2c^2r}\frac{dV(r)}{dr} \tag{2.58}$$

The $\widehat{H}_{S-O}$ term can be rewritten by using the $J^2 = (\widehat{L}^2 + \widehat{S}^2)$ relationship and the equation becomes

$$\widehat{H}_{S-O} = \frac{1}{2}f(r)\widehat{J}^2 - \widehat{L}^2 - \widehat{S}^2 \tag{2.59}$$

Noting that

$$\widehat{J}^2 - \widehat{L}^2 - \widehat{S}^2|n, j, m_j, l, s\rangle = j(j+1) - l(l+1) - s(s+1)\hbar^2\langle f(r)\rangle \tag{2.60}$$

and the expectation value of $\widehat{H}'$ is the unperturbed basis can be expressed as

$$\langle n, j, m_j, l, s|\widehat{H}_{S-O}|n, j, m_j, l, s\rangle = \frac{1}{2}j(j+1) - l(l+1) - s(s+1)|\hbar^2\langle f(r)\rangle \tag{2.61}$$

where f(r) term is independent of the angular and spin, the $f(r)$ value is

$$\langle f(r)\rangle = \frac{Z^3}{8\pi\epsilon_0 M^2 c^2}\int_0^\infty \frac{1}{r^3}|R_{nl}(r)|^2 r^2 dr \tag{2.62}$$

where Z is the effective atomic number. As a consequence of SOC, an electron in each orbital is no longer an electron with a well defined spin, radiative and non radiative transitions become weakly allowed since states are no longer pure spin-state. SOC is prominent for heavy elements.

3. RESULTS

3.1. Computational Procedure

All ground state geometries of the selected compounds have been generated by means of Density Functional Theory (DFT) by using the hybrid functional B3LYP [88, 106]. A full conformational search has been carried out for all the molecules. The metal free molecules have been treated with the 6-311G** basis set, and the 6-31G* basis set has been chosen for the other complexes. The time-dependent density functional theory (TD-DFT) has been used to model the excited states by employing the ωB97XD [97]/ 6-311G** level of theory. The accuracy of the selected functional and basis sets has been confirmed by the compatibility of the calculated absorption bands with the experimental ones. All DFT and TDDFT calculations were performed via Gaussian 09 software (E.01 version) [107] . The integral equation formalism polarizable continuum model [108] (IEF-PCM) has been utilized implicitly to take into account the solvent effect.

Based on the Franck-Condon principle, the vertical transitions from S_0 and S_1 geometries are calculated to generate the absorption and emission spectra, respectively. Furthermore, the dynamic and vibrational effects included in absorption and emission spectra have been reproduced to obtain real-like results considering vertical excitations between the ground state geometry (S_0) and the first excited state (S_1). The ωB97XD/ 6-311G** level of theory has been used to model absorption spectra, and the fluorescence spectra has been simulated by optimizing the S_1 geometry at the ωB97XD/ 6-31G* level of theory. Dynamic resolved spectra have been involved by establishing 20 initial conditions around S_0 and S_1 geometries from the Wigner distribution [109, 110] as implemented in Newton-X software package [111].

Natural Transition Orbital Analysis has been carried out with the aim of making evident the excited state topologies and evaluating the charge transfer character of the electronic transitions by using ωB97xD/6-311G** level of theory. By analyzing the occupied and virtual transition orbitals, the Φ_s index value [105, 112, 113] has been calculated by use of the NANCYEX2.0 software bundle.

Finally, in order to properly analyze the intersystem crossing probability as well as the efficiency of activating the molecular oxygen, the energy levels have been elucidated to determine the relative triplet state positions, singlet-triplet energetic gaps and spin-orbit coupling via Amsterdam Density Functional (ADF) package [114, 115]. ADF calculations have been used to the geometries generated by sampling the S_0 and S_1 geometries via Wigner Distribution, using the B3LYP functional with a slater type [116] TZP basis set for metal atom and DZP basis set for all others .

3.2. Ground State Geometries

The arrangement of organometallic complexes in three-dimensions are modelled by using DFT method with B3LYP functional, 6-31G* and 6-311G** basis sets for MPcs and H_2Pcs, respectively. There are several computational studies based on tetrapyrrole derivatives, where B3LYP functional has been used to optimize the structures [117–119]. These studies highlighted that B3LYP functional has been proved convenient for large molecule calculations.

First of all, the metal-free Pcs are optimized and then the other geometries are obtained by adding zinc metal and nickel metal to the centers of the H_2Pc geometries as displayed in Table 3.1. The spin multiplicity value of NiPcs is taken as 1. The molecular structures are primarily optimized in vacuum phase, and the resultant geometry is recalculated in water phase by using the PCM solvent model.

Concerning their molecular shapes, the non-substituted phthalocyanines (R_1-Pcs) conserve their planar structure. These results are in good agreement with the X-Ray studies of non-substituted phthalocyanines [120]. Likewise, symmetrical pentafluorobenzyloxy substituted Pcs are obtained by the introduction of electron withdrawing groups, in these cases, the ring distortion is not observed and the ring core keeps its planar shape. The fluorinated benzyl groups are orthogonal to the phthalocyanine ring.

Table 3.1. Molecular structures of non-substituted (R_1) and pentafluorobenzyloxy substituted (R_2) phthalocyanines (B3LYP/6-31G*).

R_1 substituted Pcs	R_2 substituted Pcs
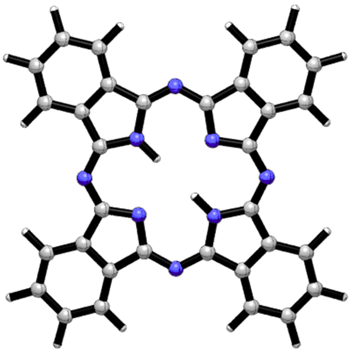 R_1-H_2Pc	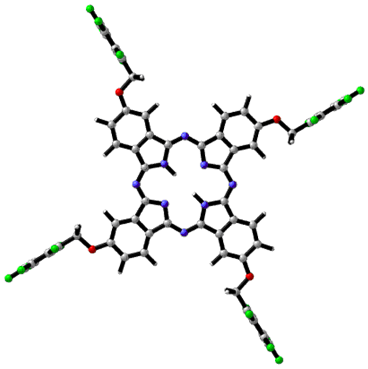 R_2-H_2Pc
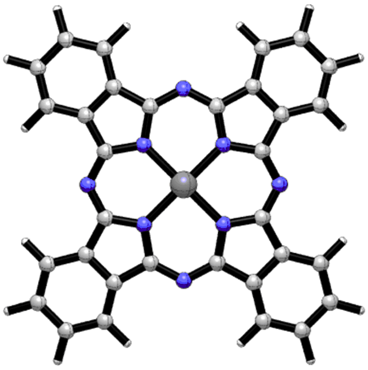 R_1-ZnPc	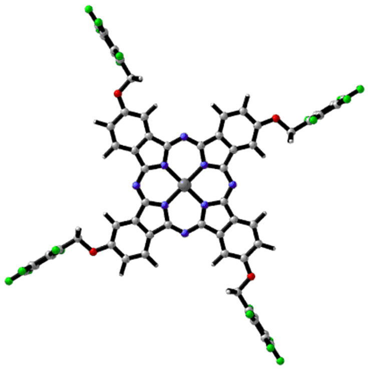 R_2-ZnPc
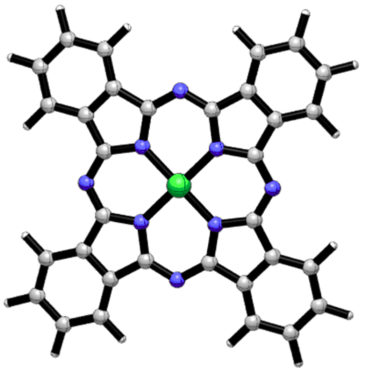 R_1-NiPc	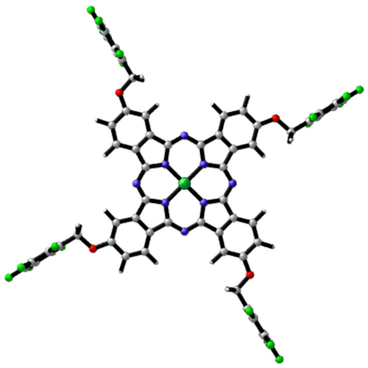 R_2-NiPc

Metal-free structures belong to D_{2h} symmetry point group with the planar phthalocyanine ring, and MPcs have the D_{4h} symmetry. These results are consistent with

Robertson's X-Ray studies [16]. Furthermore, the central atom effect on the morphology can be seen in Table 3.2 which reports the distance between two nitrogens located on two neighbor isoindole rings. If this distance in R_1-H_2Pc case is attributed to the base, the inner core of R_1-NiPc is quite smaller, on the other hand, the one in R_1-ZnPc is proportionally larger. This distinction can be explained by the size of metal atom located in the cavity, the Zn atom (r=197 pm) has larger atomic radius than Ni atom (r=125pm). Due to the fact that nuclear charge of Ni atom is almost the same as its screening effect, whereas, the nuclear charge of Zn atom is lower than the screening effects, and it causes the atomic radius to increase.

Table 3.2. The distance between two neigbour iminic nitrogen (Å) for ground state structures.

Molecules	**N-N distance in Å**
R_1-H_2Pc	2.812
R_1-ZnPc	2.815
R_1-NiPc	2.696
R_2-H_2Pc	2.807
R_2-ZnPc	2.814
R_2-NiPc	2.691

3.3. Electronic Spectra

After having geometries with their minimum energies, electronic spectra are simulated by TD-DFT method and the ωB97XD functional is employed. Since the R_2-Pcs have experimental data only in chloroform, the absorption spectra are primarily obtained in chloroform solvent in order to test the chosen methodology, comparing the calculated data with the experimental ones [121]. However, the split Q band of R_1-H_2Pc which is its specific feature, is not observed in the absorption spectrum. To overcome this issue, by using Wigner distribution function (WDF), the ground state geometries are sampled and 100 initial conditions have been generated. The calculated Q band wavelengths of R_2 substituted phthalocyanines by using 20 snapshots of the initial geometries in chloroform together with the experimental data are reported in Table 3.3.

Table 3.3. Q-Band wavelengths λ_{nm} (in parenthesis in eV) in chloroform by using ωB97XD/6-311G**//B3LYP/6-31G* of R$_2$-Pcs by using the ground state geometries sampling based on the WDF band their experimental UV/vis data in chloroform.

Molecules	Calculated		Experimental	
R$_2$-H$_2$Pc	666nm (1.86eV)	730nm (1.69eV)	663nm (1.87eV)	699nm (1.77eV)
R$_2$-ZnPc	656nm (1.89eV)		678nm (1.82eV)	
R$_2$-NiPc	636nm (1.94eV)		670nm (1.85eV)	

The experimental electronic spectrum of R$_2$-H$_2$Pc shows two distinct absorption peaks at 663nm (1.87eV) and 699 nm (1.77eV) with $\pi-\pi^*$ character. Theoretically, the split Q band shape is present at 666 nm (1.86eV) and 730 nm (1.69eV). The Q band of R$_2$-ZnPc is present at 678 nm (1.82eV) experimentally and the calculated absorption band is located at 656 nm (1.89eV). Moreover, in the case of R$_2$-NiPc, Q-Band is located at 670 nm (1.85eV) and its theoretical Q-Band is present at 636nm (1.94eV). For all 3 cases, the energies are in agreement with the experimental absorbance energies and the differences between the Q-Band wavelength data in chloroform is not larger than 0.09eV. Consequently, the protocol is proven to be capable of reproducing the experimental spectra.

3.3.1. Absorption Properties in the Q-Band Region

In photodynamic therapy, the photosensitizer (PS) is injected into the body. Since the drug is excited in body-fluid, the water-based environment may affect the vertical transition energy of PS. Because of the fact that, the excited state calculations are handled mainly in water phase to mimic the human body environment [122].

Table 3.4. Calculated static and dynamic effect included in absorption wavelengths in nm (in eV in parenthesis), (ωB97XD/6-311G** in water).

Molecules	Static (λ_{nm})	Dynamic Effects Included (λ_{nm})
R$_1$-H$_2$Pc	543 (2.28) 600 (2.06)	648 (1.91) 705 (1.75)
R$_1$-ZnPc	652 (1.90)	663 (1.87)
R$_1$-NiPc	641 (1.93)	652 (1.90)
R$_2$-H$_2$Pc	666nm (1.86)	657 (1.88) 733 (1.69)
R$_2$-ZnPc	643 (1.92)	657 (1.88)
R$_2$-NiPc	644 (1.92)	661 (1.87)

Static absorption spectra calculations are compared with the dynamic effect included spectra in Table 3.4. As observed in Table 3.4, the vibrational absorbances are red shifted In the case of R_2-H_2Pc, static calculations predict only one broad Q band at 666nm (1.86 eV), however, two distinct Q bands are present at 657nm (1.88) and 733nm (1.69 eV) in the calculations using the Wigner sampled geometries. In order to make a good prediction, vertical transitions are calculated by using the Wigner procedure as shown in Figure 3.1.

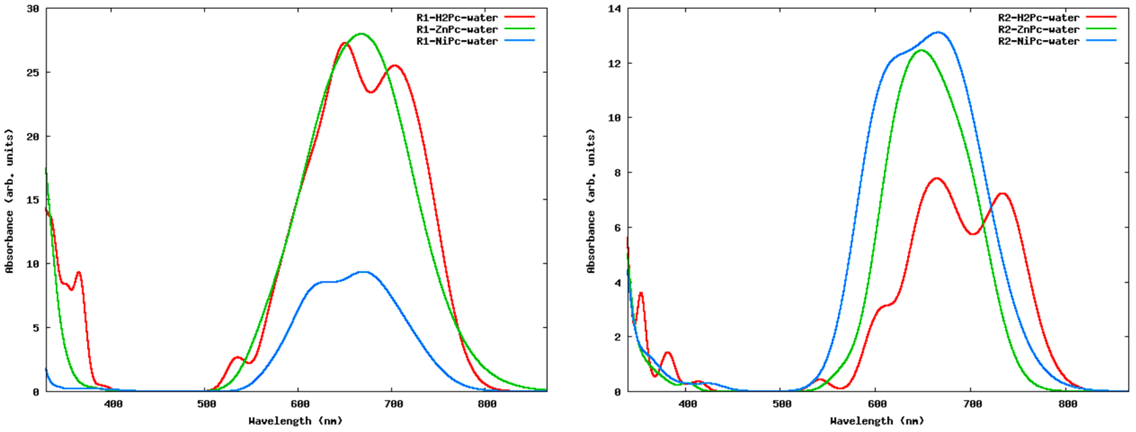

Figure 3.1. Calculated superimposed absorption spectra with dynamic effects of R_1Pcs and R_2Pcs (ωB97XD/6-311G** in water).

In Figure 3.1, for each case, two bands are clearly observed, B band and Q band and all phthalocyanines show intense Q bands ranging from 650nm to 733nm, the latter are included in the therapeutic window (650-1350nm) [123,124]. Among the R_1-substituted phthalocyanines, there is no sharp difference between their wavelengths. R_1-H_2Pc shows a split Q band at 648 nm (1.91 eV) and 705nm (1.75 eV), R_1-ZnPc has intense Q band at 663nm (1.87eV) and R_1-NiPc exhibits Q band absorbance at 652nm (1.90 eV), the latter has a hypsochromic shift, in comparison to R_1-ZnPc and R_1-H_2Pc.

Concerning the band intensity, R_1-ZnPc and R_1-H_2Pc intensities are almost identical. However, a sharp difference is observed in the case of R_1-NiPc: which has an intensity around 9 units. On the other hand, Q bands of R_2-Pcs are slightly red shifted as compared to R_1-Pcs. The only exception is R_2-ZnPc having blue shift, the band is observed at 650nm (1.88 eV). R_2-H_2Pc show two distinct Q bands at 657 nm (1.88 eV) and 733nm (1.69 eV) and R_2-NiPc's Q band is found at 661nm (1.87 eV). Concerning their band shapes, the most intense band belongs to R_2-NiPc 13 units, however, except for R_2-H_2Pc shows less intense band compared to the R_1-H_2Pc. Overall, the pentafluorobenzyloxy- subsituent effect on absorption wavelength may be ignored, but its influence on band intensity may not be underestimated.

In addition, the absorption properties depend on the solvent. For this reason, absorbance wavelengths in vacuum phase and in water are reported in Table 3.5 to shed light on environmental effect. Vacuum phase can be considered as a non-polar solvent in calculations due to not having any dipole moment. Since water is the most polar solvent, these calculations provide the effects of solvents at extrema points on the absorption features. Generally, phthalocyanine molecules exhibit longer wavelength absorption in polar solvent comparing to the non-polar environment. Exceptional cases are Zn coordinated phthalocyanines, their Q bands are blue shifted in water phase.

Table 3.5. Calculated absorption wavelengths in nm (in eV in paranthesis), at (ωB97XD/6-311G** in vacuum and in water).

Molecules	Vacuum Phase (λ_{nm})	Water Phase (λ_{nm})
R_1-H_2Pc	618 (2.00) 691 (1.79)	648 (1.91) 705 (1.75)
R_1-ZnPc	664 (1.86)	663 (1.87)
R_1-NiPc	638 (1.94)	652 (1.90)
R_2-H_2Pc	623 (1.99) 662 (1.87)	657 (1.88) 733 (1.69)
R_2-ZnPc	674 (1.83)	657 (1.88)
R_2-NiPc	634 (1.95)	661 (1.87)

3.3.2. Fluorescence Properties

In order to access the fluorescence properties, the excited singlet geometries are optimized in water by using ωB97XD with 6-31G* basis set. An excited photosensitizer molecule may return to its S_0-state via fluorescence emitting pathway [125]. However, the desirable route of PDT is a radiationless process, the transition to the triplet excited state is a prerequisite to damage cells. The strong fluorescence peak represents that the excited molecule tends to return its ground state position instead of undergoing the intersystem crossing.

In addition to photodynamic therapy, a photosensitizer having strong fluorescence emission in near-infrared (NIR) region (650-900 nm), can be used in fluorescence imaging cancer as a diagnosis agent [126–128]. It is well known that dyes that emit in the NIR are more favorable for biological imaging thanks to their ability of minimizing the environmentally-induced light scattering. Not to mention to fact that, PS accumulating the cancerous cells provides the well-suited detection of tumors and help to distinguish them from healthy tissues by emitting the light.

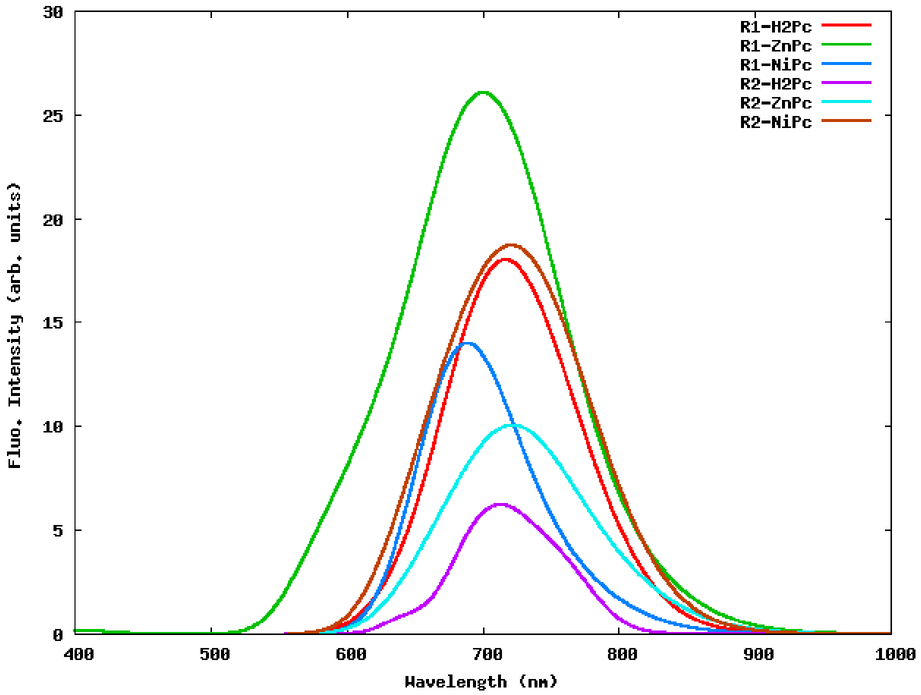

Figure 3.2. Calculated superimposed emission spectra via Wigner procedure (ωB97XD/6-31G* in water).

In Figure 3.2, the calculated fluorescence emissions by sampling S_1 geometries based on the WDF, are superimposed. R_2 and R_1Pcs exhibit fluorescence emission at around 700nm which is covered in Near-Infrared region (NIR). Since the intensity gives an idea about the decay of excited molecules to the ground state, less intense peak may be a clue of the intersystem crossing process. R_2-H_2Pc shows the weakest fluorescence with 6.2 units intensity at around 713nm (1.73 eV) and R_1-ZnPc displays the strongest emission with 26 units fluorescence intensity at 700nm (1.77eV).

Table 3.6. Calculated excitation and emission spectral data and Stokes shifts (ωB97XD/6-31G* in water).

Molecules	$S_0 \rightarrow S_1$ λ_{exc} (nm)	$S_1 \rightarrow S_0$ λ_{ems} (nm)	Stokes Shifts ΔS (x10^5 cm^{-1})
R_1-H_2Pc	599	790	52.35
R_1-ZnPc	653	780	78.74
R_1-NiPc	654	740	11.62
R_2-H_2Pc	670	792	81.96
R_2-ZnPc	629	764	74.07
R_2-NiPc	642	650	1.25

On the other hand, as stated before, PS are also useful as NIR diagnosis agent. A fluorophore having large Stokes shift (ΔS) is much easier to use as a visualization agent then a fluorophore having a small ΔS. The calculated Stokes shifts by using static approach, are reported in Table 3.6. R_1-H_2Pc, R_1-ZnPc, R_2-H_2Pc and R_2-ZnPc have ΔS values respectively, 52.35x10^5 cm^{-1}, 78.74x10^5 cm^{-1}, 81.96x10^5 cm^{-1} and 74.07x10^5 cm^{-1}. The one with high ΔS value with high emission intensity is a good candidate for NIR diagnosis agent.

3.4. Natural Transition Orbitals

The excited state nature of molecules, the vertical transitions $S_0 \rightarrow S_1$, $S_0 \rightarrow S_2$, $S_0 \rightarrow S_3$ and $S_0 \rightarrow S_4$ are studied by means of Natural Transition Orbitals (NTO). The occupied natural transition orbitals (oNTO), virtual natural transition orbitals (vNTO) and corresponding quantum descriptor ϕ_s and oscillator strengths (f) are reported in Table 3.7 to Table 3.12. The calculations are performed at ωB97XD/6-311G**// B3LYP/6-31G* level of theory, by taking into account the water solvent implicitly.

Table 3.7. Occupied and virtual NTO's and corresponding ϕ_s values of R_1-H_2Pc.

Transitions	oNTO	vNTO
$S_0 \rightarrow S_1$ $\phi_s = 0.8683$ f= 0.6107	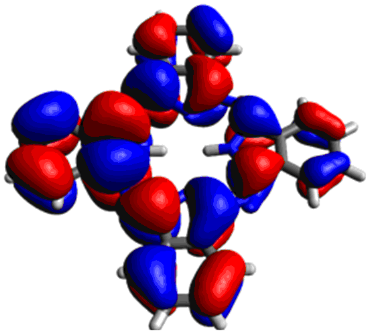	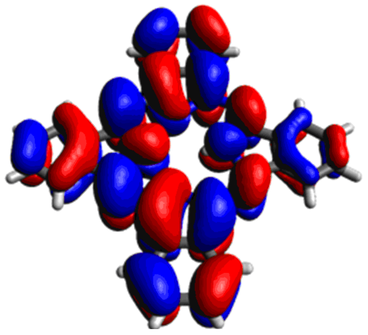
$S_0 \rightarrow S_2$ $\phi_s = 0.7413$ f= 0.5847	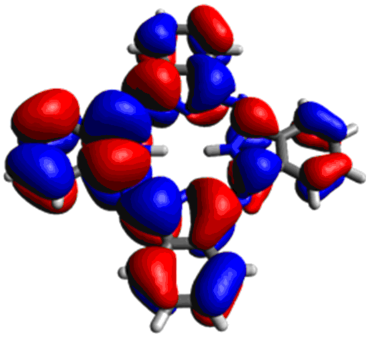	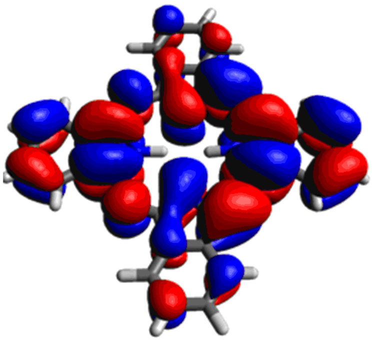
$S_0 \rightarrow S_3$ $\phi_s = 0.7094$ f= 0.1628	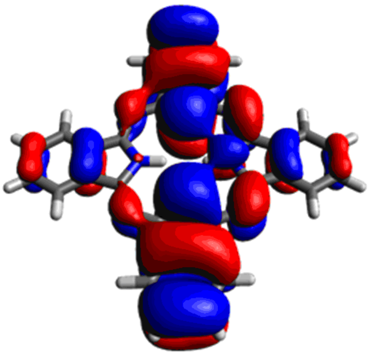	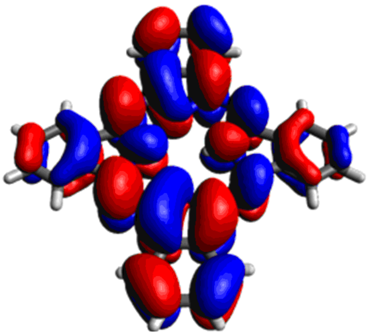
$S_0 \rightarrow S_4$ $\phi_s = 0.7107$ f= 0.0321	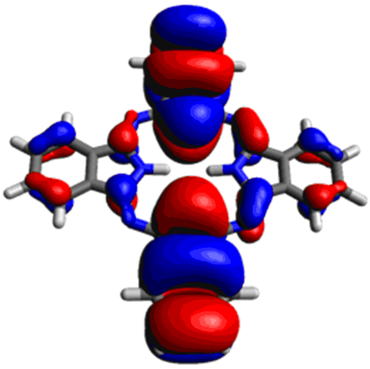	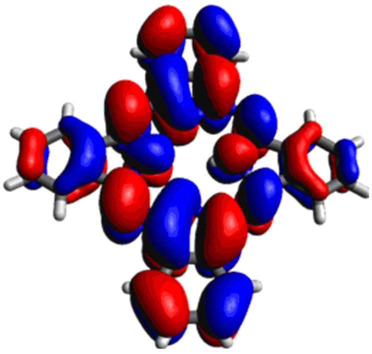

Table 3.8. Occupied and virtual NTO's and corresponding ϕ_s values of R_1-ZnPc.

Transitions	oNTO	vNTO
$S_0 \rightarrow S_1$ $\phi_s = 0.9087$ f= 0.6357	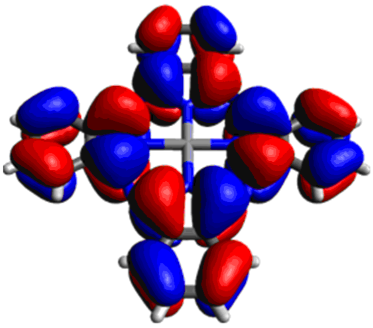	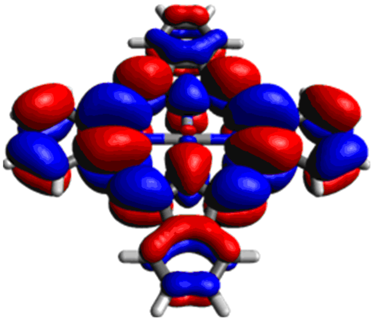
$S_0 \rightarrow S_2$ $\phi_s = 0.9087$ f= 0.6356	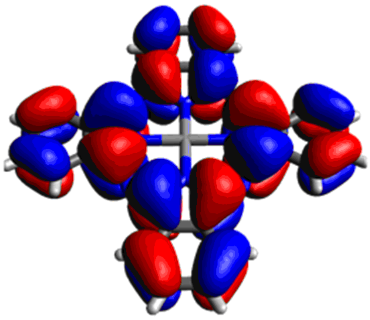	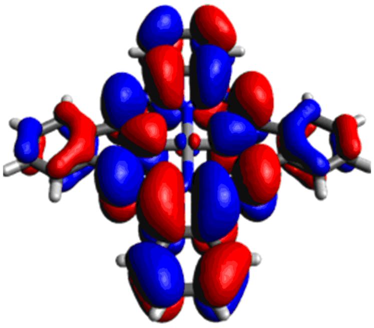
$S_0 \rightarrow S_3$ $\phi_s = 0.0571$ f= 0.000	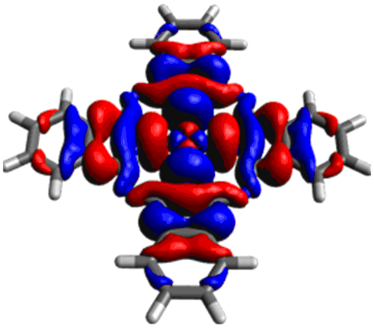	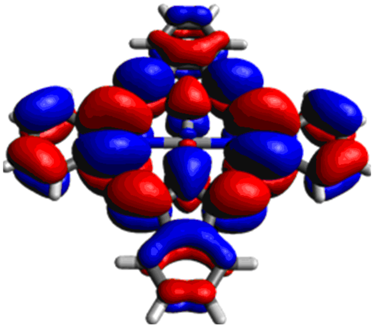
$S_0 \rightarrow S_4$ $\phi_s = 0.0570$ f= 0.000	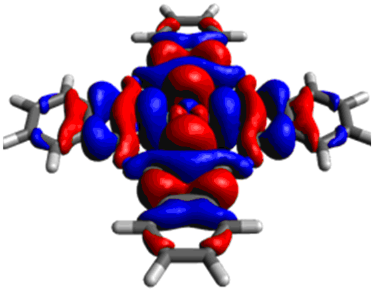	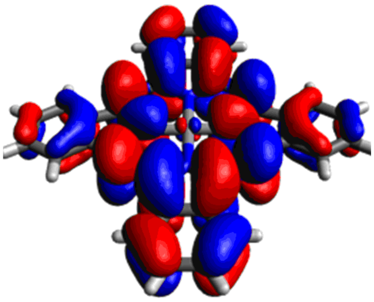

Table 3.9. Occupied and virtual NTO's and corresponding ϕ_s values of R_1-NiPc.

Transitions	oNTO	vNTO
$S_0 \rightarrow S_1$ ϕ_s = 0.7235 f= 0.000	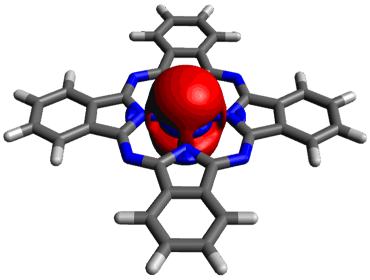	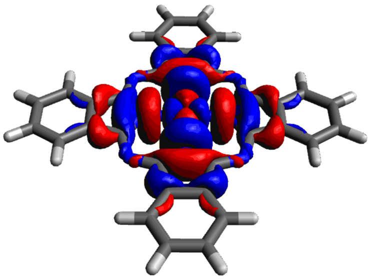
$S_0 \rightarrow S_2$ ϕ_s = 0.8694 f= 0.6080	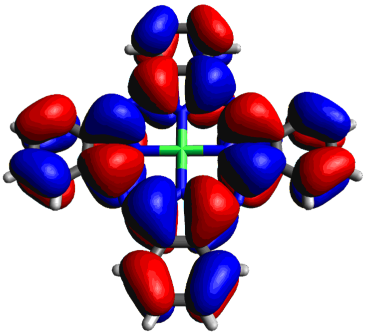	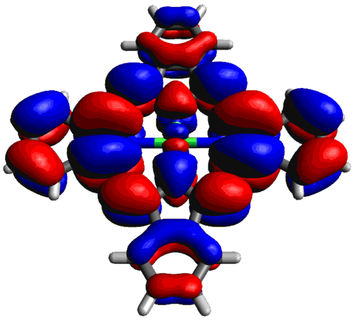
$S_0 \rightarrow S_3$ ϕ_s = 0.8694 f= 0.6080	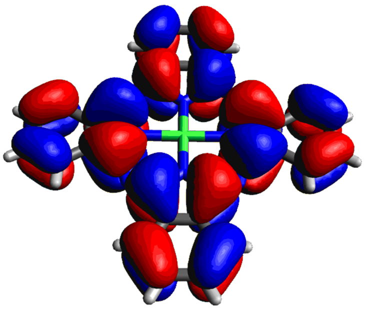	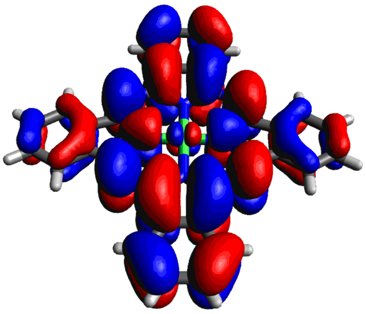
$S_0 \rightarrow S_4$ ϕ_s = 0.0870 f= 0.000	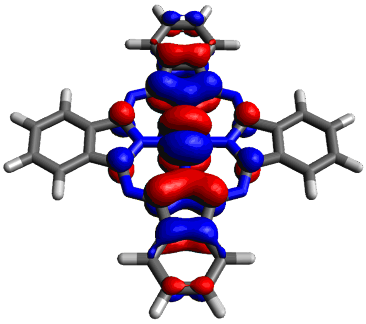	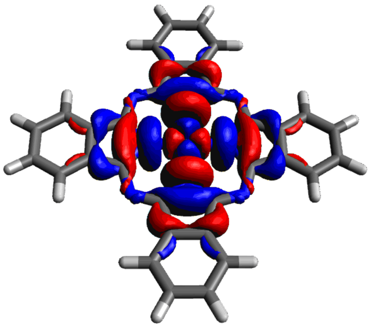

Table 3.10. Occupied and virtual NTO's and corresponding ϕ_s values of R_2-H_2Pc.

Transitions	oNTO	vNTO
$S_0 \rightarrow S_1$ $\phi_s = 0.8791$ f= 0.6753	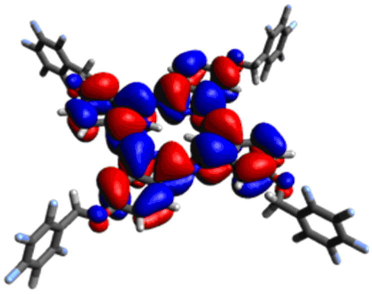	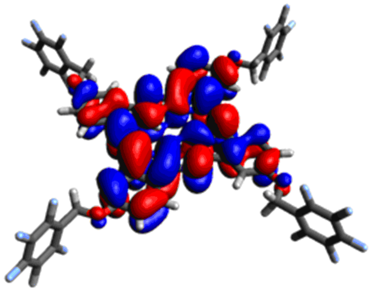
$S_0 \rightarrow S_2$ $\phi_s = 0.8873$ f= 0.7303	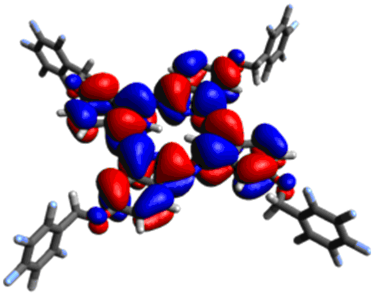	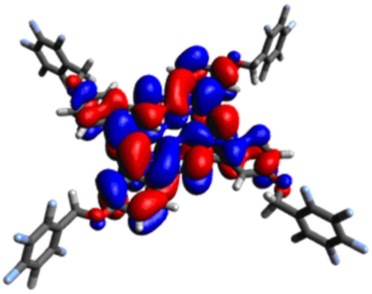
$S_0 \rightarrow S_3$ $\phi_s = 0.6218$ f= 0.1330	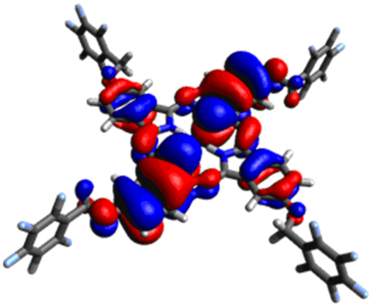	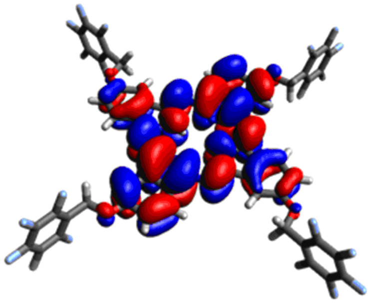
$S_0 \rightarrow S_4$ $\phi_s = 0.5475$ f= 0.000	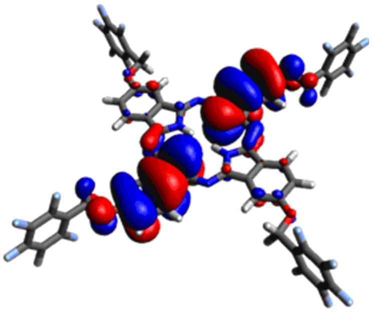	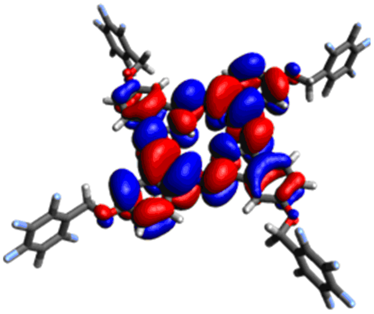

Table 3.11. Occupied and virtual NTO's and corresponding ϕ_s values of R_2-ZnPc.

Transitions	oNTO	vNTO
$S_0 \rightarrow S_1$ $\phi_s = 0.8899$ f= 0.7214	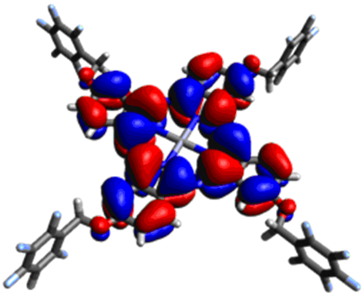	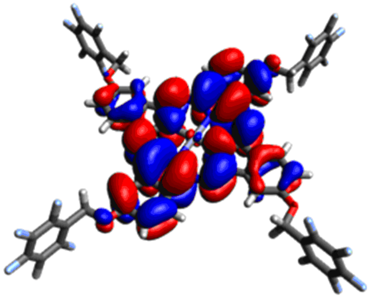
$S_0 \rightarrow S_2$ $\phi_s = 0.8900$ f= 0.7214	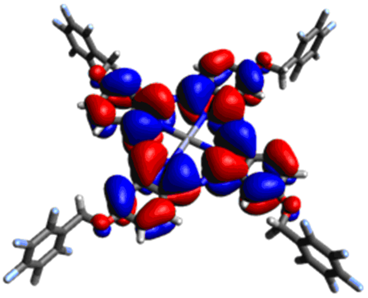	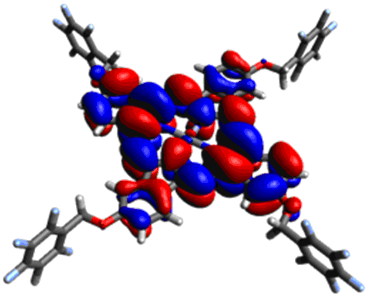
$S_0 \rightarrow S_3$ $\phi_s = 0.0534$ f= 0.000	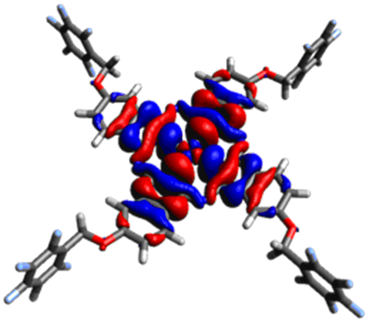	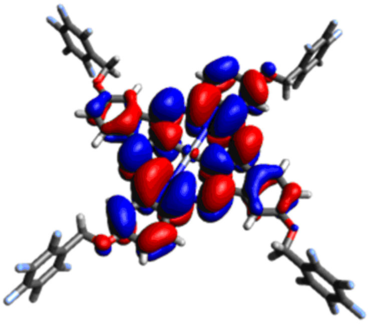
$S_0 \rightarrow S_4$ $\phi_s = 0.0533$ f= 0.000	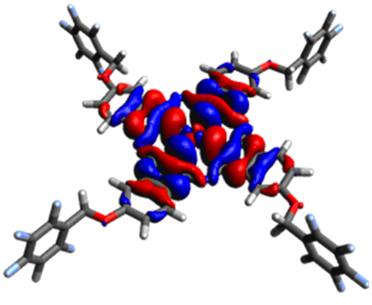	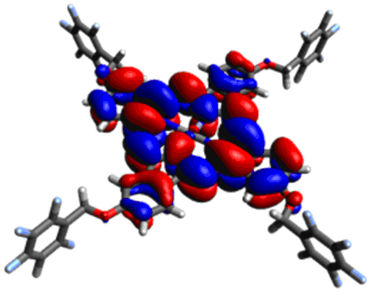

Table 3.12. Occupied and virtual NTO's and corresponding ϕ_s values of R_2-NiPc.

Transitions	oNTO	vNTO
$S_0 \rightarrow S_1$ $\phi_s = 0.8509$ f= 0.6834	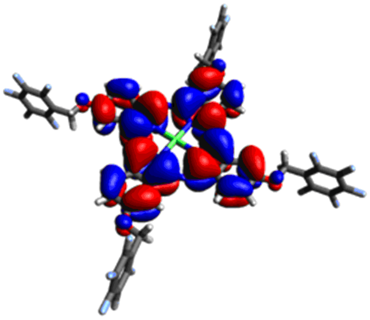	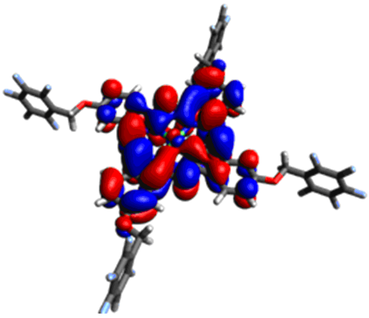
$S_0 \rightarrow S_2$ $\phi_s = 0.8509$ f= 0.6834	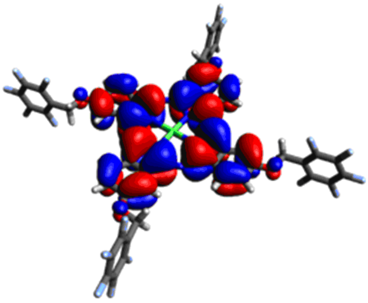	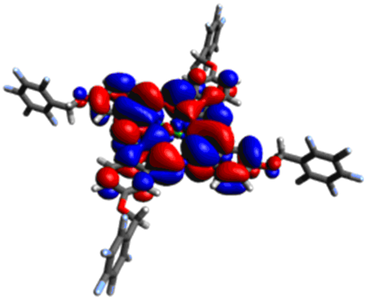
$S_0 \rightarrow S_3$ $\phi_s = 0.0976$ f= 0.000	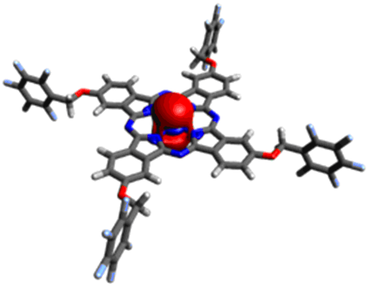	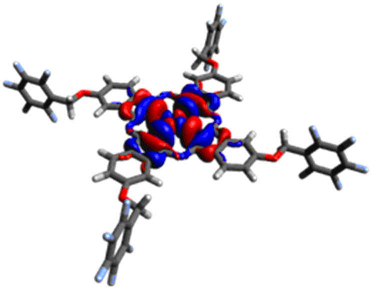
$S_0 \rightarrow S_4$ $\phi_s = 0.0915$ f= 0.000	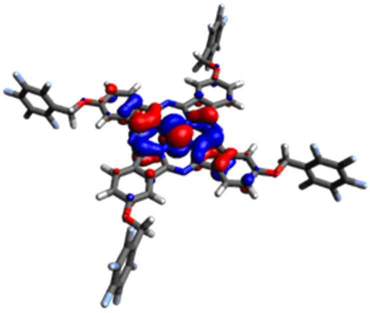	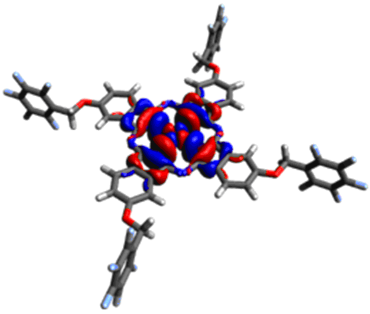

In NTO analysis, the deficiency in electronic density caused by absorption is represented as detachment matrix, and the other matrix, called attachment, represents the increase in electron density in the excite state. A transition between energy levels can be identified qualitatively by using these two matrices. Moreover, the ϕ_s index which describes quantitatively the photoinduced electronic charge density variation and it is obtained from the overlap value of the matrices. A detailed mathematical explanation of Detachment/Attachment matrices can be found in Natural Transition Orbitals section under the Methodology chapter. As a reminder the charge transfer character corresponds to a ϕ_s index close to 0. Furthermore, f stands for oscillator strengths which is a description of the population of excited molecules.

The first vertical transition ($S_0 \rightarrow S_1$) of almost all molecules have π-π^* transition character as previously shown in absorption spectra, these transitions are mostly located on the phthalocyanine ring. Some transitions have ϕ_s value closer to the zero in metal coordinated systems, but unfortunately, these transitions do not show oscillator strength. So these states are not populated, then they may be ignored. In R_2 substituted phthalocyanines, the additional pentafluorobenzyloxy group participation is insignificant. Because of the fact that, the electron density is mainly distributed over the phthalocyanine core ring, not on the fluorinated benzyloxy part.

3.5. Energy Levels

As studied in previous sections, the molecules are efficiently promoted to the excited state. Two different starting geometries, ground state and excited state, are used to describe the energy levels of each molecule. The energy levels of ground state and excited state are shown in Figure 3.3 and Figure 3.4, and their corresponding energies are listed in Table 3.13 and Table 3.14, respectively. Note that these energy levels are calculated by using 20 randomly generated geometries via Wigner distribution around ground state (S_0) and excited state (S_1) structures and the energy levels are determined by the mean values together with the standard deviations. The difference between the data collected in Table 3.13 and Table 3.14 is generally around 0.07eV. In some cases the dissimilarity is found to be larger, but not above 0.21eV.

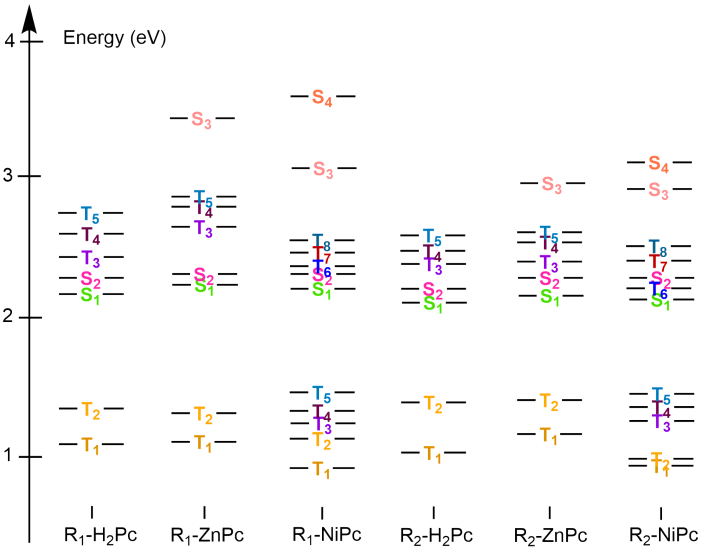

Figure 3.3. Schematic illustration of energy diagrams by using S_0 geometry (B3LYP/DZP in water).

Table 3.13. Singlet and Triplet State Energies (in eV) around ground state geometry (S_0) (B3LYP/DZP in water).

	R_1Pcs			R_2Pcs		
	H_2Pc	**ZnPc**	**NiPc**	**H_2Pc**	**ZnPc**	**NiPc**
T_8			2.471±0.08			2.392±0.08
T_7			2.406±0.09			2.325±0.07
T_6			2.321±0.10			2.240±0.07
T_5	2.765 ± 0.12	2.853 ± 0.05	1.452±0.06	2.592±0.09	2.609±0.09	1.449±0.06
T_4	2.630±0.14	2.805±0.06	1.320±0.08	2.468±0.08	2.538±0.10	1.322±0.08
T_3	2.468±0.18	2.706±0.08	1.260±0.08	2.371±0.10	2.382±0.11	1.246±0.09
T_2	1.368±0.07	1.376±0.08	1.139±0.07	1.345±0.10	1.368±0.05	0.970±0.16
T_1	1.100±0.09	1.126±0.08	0.965±0.12	1.066±0.09	1.166±0.06	0.960±0.14
S_4			3.649±0.16			3.175±0.15
S_3		3.571±0.14	3.113±0.64		2.975±0.14	2.898±0.31
S_2	2.281±0.04	2.299±0.02	2.292±0.03	2.236±0.05	2.267±0.04	2.264±0.04
S_1	2.175±0.04	2.221±0.03	2.204±0.03	2.129±0.04	2.197±0.04	2.177±0.05

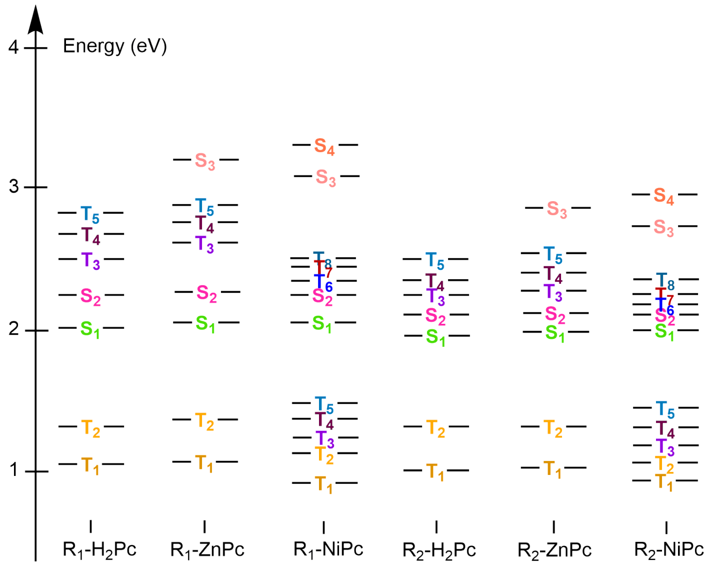

Figure 3.4. Schematic illustration of energy diagrams by using S_1 geometry (B3LYP/DZP in water).

Table 3.14. Singlet and Triplet State Energies (in eV) around excited state geometry (S_1) (B3LYP/DZP in water).

	R$_1$Pcs			R$_2$Pcs		
	H$_2$Pc	**ZnPc**	**NiPc**	**H$_2$Pc**	**ZnPc**	**NiPc**
T$_8$			2.499±0.06			2.388±0.08
T$_7$			2.423±0.09			2.292±0.08
T$_6$			2.332±0.07			2.201±0.11
T$_5$	2.808±0.08	2.821±0.08	1.475±0.10	2.503±0.08	2.539±0.10	1.494±0.08
T$_4$	2.701±0.07	2.744±0.10	1.389±0.10	2.389±0.10	2.470±0.10	1.337±0.12
T$_3$	2.515±0.13	2.638±0.08	1.326±0.10	2.261±0.12	2.334±0.13	1.259±0.11
T$_2$	1.355±0.10	1.394±0.11	1.118±0.09	1.353±0.12	1.401±0.09	1.084±0.10
T$_1$	1.042±0.07	1.035±0.11	0.972±0.09	1.042±0.08	1.016±0.09	0.931±0.13
S$_4$			3.515±0.31			2.965±0.30
S$_3$		3.460±0.18	3.242±0.49		2.940±0.16	2.737±0.39
S$_2$	2.171±0.07	2.192±0.05	2.210±0.05	2.149±0.06	2.179±0.10	2.173±0.05
S$_1$	2.020±0.05	2.047±0.05	2.059±0.03	1.984±0.05	1.994±0.05	2.00±0.05

One can notice the energy diagram difference between complexes. Nickel coordinated phthalocyanines have quite low triplet energies (T_3, T_4 and T_5), their T_5 levels are below their S_1 states and they are around 1.46eV. For this reason, additional triplet energy levels are calculated for these two. Moreover, the reported in NTO calculations, Ni coordinated and Zn coordinated cases show metal participation above the second excited singlet state. Because of the fact that, additional singlet states are calculated. In general, the lowest lying excited singlet level is found around 2.0eV in each cases and the ensuing singlet level is quite closer to it. The calculated S_3 values are above 3.00 eV except for the R_2-NiPc case.

Moreover, the ability to generate $^1O_2$ is indicated by triplet energy (E_T) which makes a photosensitizer favorable to PDT. The threshold value of the lowest lying triplet state is 0.98eV for efficient energy transfer to promote the molecular oxygen ($^3\Sigma_g$) to the singlet oxygen ($^1\Delta_g$) [129]. In Table 3.14, the T_1 states have energies above this treshold energy value. The lowest triplet state, R_2NiPc is located around 0.931 eV and R_1NiPc is around 0.972 eV which are below the limit. Therefore, the essential condition to produce singlet oxygen is fulfilled by the studied phthalocyanines except for the R_2NiPc.

Despite the fact that the triplet excite state is precondition for obtaining cytotoxic singlet oxygen, it can only be populated by intersystem crossing process. For that reason, since ISC transition may occur from an excited singlet state to an excited triplet state, the energy levels are identifed in order to specify the potential ISC pathways. The excited molecule may undergo ISC, either from the lowest lying excited states which is a direct mechanism, or from a singlet excited state to the triplet state which lays close energetically to the singlet state, called indirect mechanism [130]. The intersystem crossing probability will be scrutinized in the next section.

3.6. Intersystem Crossing Probability

Intersystem crossing (ISC) is in competition with the other relaxation process, fluorescence. ISC is a non-radiative route from singlet to triplet excited states that is favored by two factors: one of them is the singlet-triplet energy separation and the other is the spin-orbit coupling. The latter phenomena depends upon the spin-orbit coupling (SOC). A higher SOC favors the transition probability. Additionally, it is exponentially dependent on the energy difference. When the energy gap is small, the probability of transition is larger [131, 132].

In photochemistry, the ISC plays a key role due to the fact that, the only pathway to populate triplet state is ISC transition. In order to consider the intersystem crossing probability, the energy separations and also, spin-orbit coupling constants are calculated by means of B3LYP functional with the TZP basis set for metal atoms and DZP for all others. The calculations are done by using the generated 20 geometries via Wigner distribution sampled around both ground state and excited state. The energy separation (Δ_{ST}) of each singlet-triplet states is determined by substracting the energies reported in Table 3.13 and Table 3.14. The spin-orbit coupling constants (SOCC) are calculated for each singlet triplet states.In Figure 3.5 and Figure 3.6, the mean values of ST Gap (in eV) and SOCC (cm^{-1}), together with their standard deviations are reported.

As stated before, the accumulation on the triplet state is strongly dependent on the possibility of excited molecule to undergo ISC. However, in the case of large energy separations between the excited singlet and triplet states, the excited molecule may prefer to emit its energy as fluorescence instead of following the ISC to the triplet manifold. Moreover, the other factor, spin-orbit coupling constant (SOCC) is a variable depending on the molecules. Since the spin-orbit coupling formula has an effective atomic charge term (Z_{eff}), it increases as the power of Z_{eff} and this indicates that SOC interactions are substantially larger for atoms that are located in the bottom part of the periodic table.The spin-orbit coupling constant (SOCC) determines the magnitude of SOC between a pair of states.For that reason, the lowest energy separation between singlet and triplet states are illustrated in Figure 3.5 for R_1-Pcs and Figure 3.6 for R_2-Pcs, together with their ST gaps and SOCCs.

R_1-H_2Pc has narrow gaps which are S_1-T_3, S_1-T_2, S_2-T_3 and S_2-T_4. R_1-H_2Pc has around 0.25cm^{-1} value for SOC constant, which is moderate for the intersystem crossing. The excited R_1-H_2Pc molecule may follow indirect ISC pathways:

- $S_2 \rightarrow T_3 \rightarrow T_2 \rightarrow T_1$. The gap between S_2 and T_3 is 0.186 eV, the SOC constant is calculated 0.146 cm^{-1}.
- $S_1 \rightarrow T_2 \rightarrow T_1$. The gap is found 0.669eV and the corresponding SOCC value is 0.269 cm^{-1}.

R_1-ZnPc has satisfactory SOCC values. The highest SOCC values are identified for the transitions from S_3, however, it is not populated. Therefore, the channel to populate triplet state may be suggested as:

- $S_2 \rightarrow T_3 \rightarrow T_2 \rightarrow T_1$, the gap between S_2-T_3 is 0.446eV with 0.693 cm^{-1} of SOCC.
- $S_1 \rightarrow T_3 \rightarrow T_2 \rightarrow T_1$. S_1-T_3 gap is calculated 0.591eV and the SOCC is 1.633 cm^{-1}.

For R_1-NiPc has triplet states which are interpenetrating with singlet states and it shows excessive spin orbit couplings due to the heavy atom effect. R_1-NiPc may follow:

- $S_3 \rightarrow T_8 \rightarrow T_7 \rightarrow T_6 \rightarrow T_5 \rightarrow T_4 \rightarrow T_3 \rightarrow T_2 \rightarrow T_1$, S_3-T_8 has 0.743 eV energy difference and 17.085 cm^{-1} SOCC.
- $S_2 \rightarrow T_6 \rightarrow T_5 \rightarrow T_4 \rightarrow T_3 \rightarrow T_2 \rightarrow T_2$. 0.122eV is calculated for the separation of S_2-T_6, the SOCC is 18.483 cm^{-1}.
- $S_2 \rightarrow T_7 \rightarrow T_6 \rightarrow T_5 \rightarrow T_4 \rightarrow T_3 \rightarrow T_2 \rightarrow T_2$. 0.212eV is calculated for the separation of S_2-T_7, the SOCC is 13.989 cm^{-1}.

R_2-H_2Pc has three narrow gaps which are S_1-T_2, S_1-T_3 and S_2-T_3. However, the SOCC value is slight for the S_1-T_3 and S_2-T_3 transitions The ISC pathway of R_2-H_2Pc may be proposed as

- $S_1 \rightarrow T_2 \rightarrow T_1$. S_1-T_2 difference is 0.630 eV with 0.236 cm^{-1} SOCC value.

Additionally, R_2-ZnPc has 2 possible channel. The most probable ISC relaxations are:

- $S_2 \rightarrow T_3 \rightarrow T_2 \rightarrow T_1$. S_2-T_3 difference is 0.155 eV with 0.579 cm^{-1} SOCC value.
- $S_1 \rightarrow T_2 \rightarrow T_1$. The separation between S_1 and T_2 is 0.592 eV with 1.633 cm^{-1} SOCC value.

R_2-NiPc has several narrow gaps, and it exhibits outstanding SOCCs. The possible pathways may be suggested as:

- $S_1 \rightarrow T_5 \rightarrow T_4 \rightarrow T_3 \rightarrow T_2 \rightarrow T_1$. The gap between S_1-T_5 is 0.507 eV and SOCC value is calculated 9.187 cm^{-1}.
- $S_1 \rightarrow T_6 \rightarrow T_5 \rightarrow T_4 \rightarrow T_3 \rightarrow T_2 \rightarrow T_1$.$S_1$-$T_6$ has 0.199eV difference, 17.296 cm^{-1} is obtained for the SOCC.
- $S_1 \rightarrow T_7 \rightarrow T_6 \rightarrow T_5 \rightarrow T_4 \rightarrow T_3 \rightarrow T_2 \rightarrow T_1$. S_1-T_7 has 0.290 eV energy separation with 12.058 cm^{-1} coupling value.
- $S_2 \rightarrow T_6 \rightarrow T_5 \rightarrow T_4 \rightarrow T_3 \rightarrow T_2 \rightarrow T_1$. The separation between S_2-T_6 is quite narrow, 0.027eV. The calculated SOCC is 13.515 cm^{-1}.
- $S_2 \rightarrow T_7 \rightarrow T_6 \rightarrow T_5 \rightarrow T_4 \rightarrow T_3 \rightarrow T_2 \rightarrow T_1$. The S_2-T_7 gap is 0.119 eV and the transition has 15.765 cm^{-1} SOCC value.

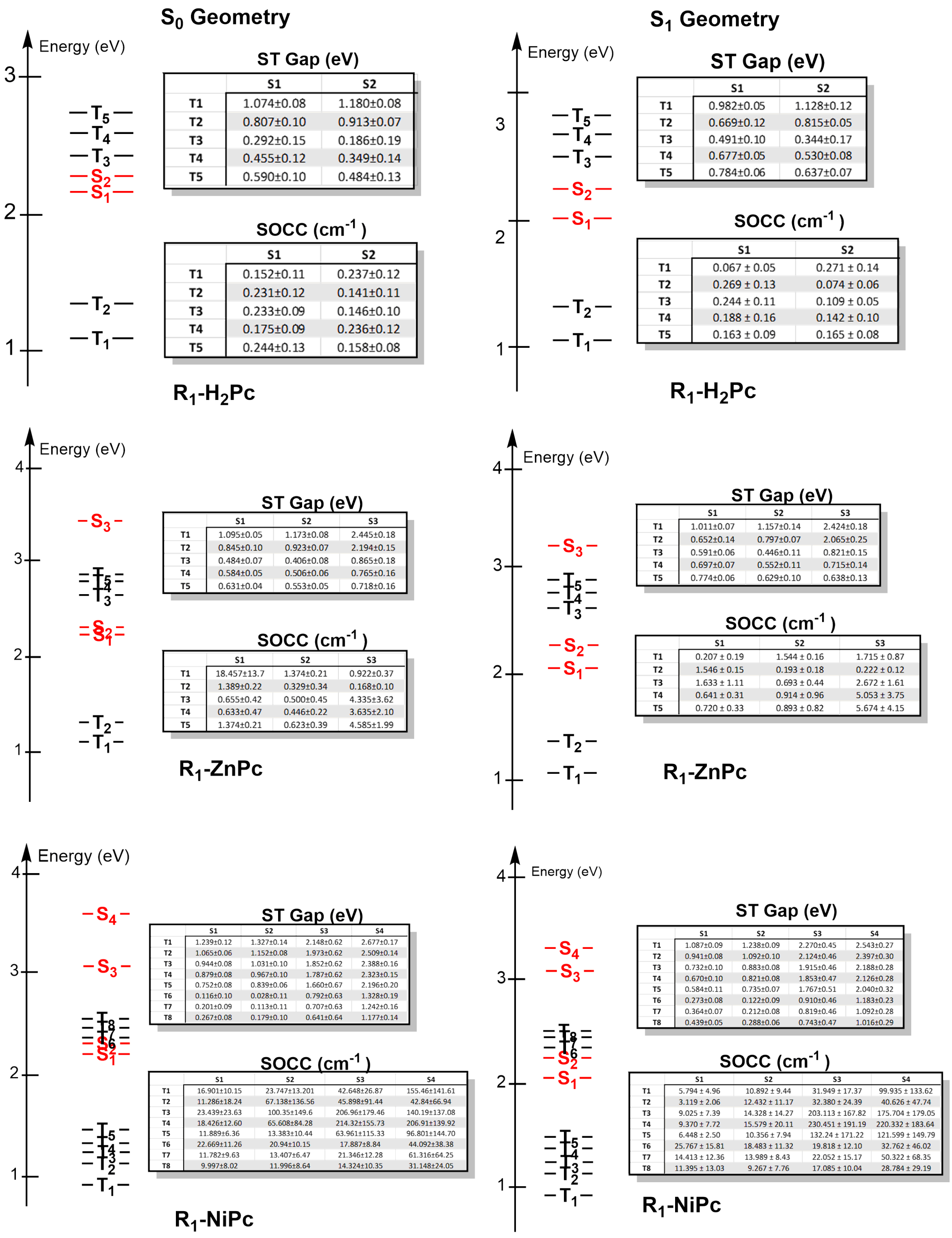

S_0 Geometry

ST Gap (eV)

	S1	S2
T1	1.074±0.08	1.180±0.08
T2	0.807±0.10	0.913±0.07
T3	0.292±0.15	0.186±0.19
T4	0.455±0.12	0.349±0.14
T5	0.590±0.10	0.484±0.13

SOCC (cm^{-1})

	S1	S2
T1	0.152±0.11	0.237±0.12
T2	0.231±0.12	0.141±0.11
T3	0.233±0.09	0.146±0.10
T4	0.175±0.09	0.236±0.12
T5	0.244±0.13	0.158±0.08

R_1-H_2Pc

S_1 Geometry

ST Gap (eV)

	S1	S2
T1	0.982±0.05	1.128±0.12
T2	0.669±0.12	0.815±0.05
T3	0.491±0.10	0.344±0.17
T4	0.677±0.05	0.530±0.08
T5	0.784±0.06	0.637±0.07

SOCC (cm^{-1})

	S1	S2
T1	0.067 ± 0.05	0.271 ± 0.14
T2	0.269 ± 0.13	0.074 ± 0.06
T3	0.244 ± 0.11	0.109 ± 0.05
T4	0.188 ± 0.16	0.142 ± 0.10
T5	0.163 ± 0.09	0.165 ± 0.08

R_1-H_2Pc

ST Gap (eV)

	S1	S2	S3
T1	1.095±0.05	1.173±0.08	2.445±0.18
T2	0.845±0.10	0.923±0.07	2.194±0.15
T3	0.484±0.07	0.406±0.08	0.865±0.18
T4	0.584±0.05	0.506±0.06	0.765±0.16
T5	0.631±0.04	0.553±0.05	0.718±0.16

SOCC (cm^{-1})

	S1	S2	S3
T1	18.457±13.7	1.374±0.21	0.922±0.37
T2	1.389±0.22	0.329±0.34	0.168±0.10
T3	0.655±0.42	0.500±0.45	4.335±3.62
T4	0.633±0.47	0.446±0.22	3.635±2.10
T5	1.374±0.21	0.623±0.39	4.585±1.99

R_1-ZnPc

ST Gap (eV)

	S1	S2	S3
T1	1.011±0.07	1.157±0.14	2.424±0.18
T2	0.652±0.14	0.797±0.07	2.065±0.25
T3	0.591±0.06	0.446±0.11	0.821±0.15
T4	0.697±0.07	0.552±0.11	0.715±0.14
T5	0.774±0.06	0.629±0.10	0.638±0.13

SOCC (cm^{-1})

	S1	S2	S3
T1	0.207 ± 0.19	1.544 ± 0.16	1.715 ± 0.87
T2	1.546 ± 0.15	0.193 ± 0.18	0.222 ± 0.12
T3	1.633 ± 1.11	0.693 ± 0.44	2.672 ± 1.61
T4	0.641 ± 0.31	0.914 ± 0.96	5.053 ± 3.75
T5	0.720 ± 0.33	0.893 ± 0.82	5.674 ± 4.15

R_1-ZnPc

ST Gap (eV)

	S1	S2	S3	S4
T1	1.239±0.12	1.327±0.14	2.148±0.62	2.677±0.17
T2	1.065±0.06	1.152±0.08	1.973±0.62	2.509±0.14
T3	0.944±0.08	1.031±0.10	1.852±0.62	2.388±0.16
T4	0.879±0.08	0.967±0.10	1.787±0.62	2.323±0.15
T5	0.752±0.08	0.839±0.06	1.660±0.67	2.196±0.20
T6	0.116±0.10	0.028±0.11	0.792±0.63	1.328±0.19
T7	0.201±0.09	0.113±0.11	0.707±0.63	1.242±0.16
T8	0.267±0.08	0.179±0.10	0.641±0.64	1.177±0.14

SOCC (cm^{-1})

	S1	S2	S3	S4
T1	16.901±10.15	23.747±13.201	42.648±26.87	155.46±141.61
T2	11.286±18.24	67.138±136.56	45.898±91.44	42.84±66.94
T3	23.439±23.63	100.35±149.6	206.96±179.46	140.19±137.08
T4	18.426±12.60	65.608±84.28	214.32±155.73	206.91±139.92
T5	11.889±6.36	13.383±10.44	63.961±115.33	96.801±144.70
T6	22.669±11.26	20.94±10.15	17.887±8.84	44.092±38.38
T7	11.782±9.63	13.407±6.47	21.346±12.28	61.316±64.25
T8	9.997±8.02	11.996±8.64	14.324±10.35	31.148±24.05

R_1-NiPc

ST Gap (eV)

	S1	S2	S3	S4
T1	1.087±0.09	1.238±0.09	2.270±0.45	2.543±0.27
T2	0.941±0.08	1.092±0.10	2.124±0.46	2.397±0.30
T3	0.732±0.10	0.883±0.08	1.915±0.46	2.188±0.28
T4	0.670±0.10	0.821±0.08	1.853±0.47	2.126±0.28
T5	0.584±0.11	0.735±0.07	1.767±0.51	2.040±0.32
T6	0.273±0.08	0.122±0.09	0.910±0.46	1.183±0.23
T7	0.364±0.07	0.212±0.08	0.819±0.46	1.092±0.28
T8	0.439±0.05	0.288±0.06	0.743±0.47	1.016±0.29

SOCC (cm^{-1})

	S1	S2	S3	S4
T1	5.794 ± 4.96	10.892 ± 9.44	31.949 ± 17.37	99.935 ± 133.62
T2	3.119 ± 2.06	12.432 ± 11.17	32.380 ± 24.39	40.626 ± 47.74
T3	9.025 ± 7.39	14.328 ± 14.27	203.113 ± 167.82	175.704 ± 179.05
T4	9.370 ± 7.72	15.579 ± 20.11	230.451 ± 191.19	220.332 ± 183.64
T5	6.448 ± 2.50	10.356 ± 7.94	132.24 ± 171.22	121.599 ± 149.79
T6	25.767 ± 15.81	18.483 ± 11.32	19.818 ± 12.10	32.762 ± 46.02
T7	14.413 ± 12.36	13.989 ± 8.43	22.052 ± 15.17	50.322 ± 68.35
T8	11.395 ± 13.03	9.267 ± 7.76	17.085 ± 10.04	28.784 ± 29.19

R_1-NiPc

Figure 3.5. Singlet-Triplet Separations (ST Gap) and Spin-Orbit Coupling Constants (SOCC) of R_1Pcs by using geometries of S_0 geometry and S_1 geometry (B3LYP/DZP in water).

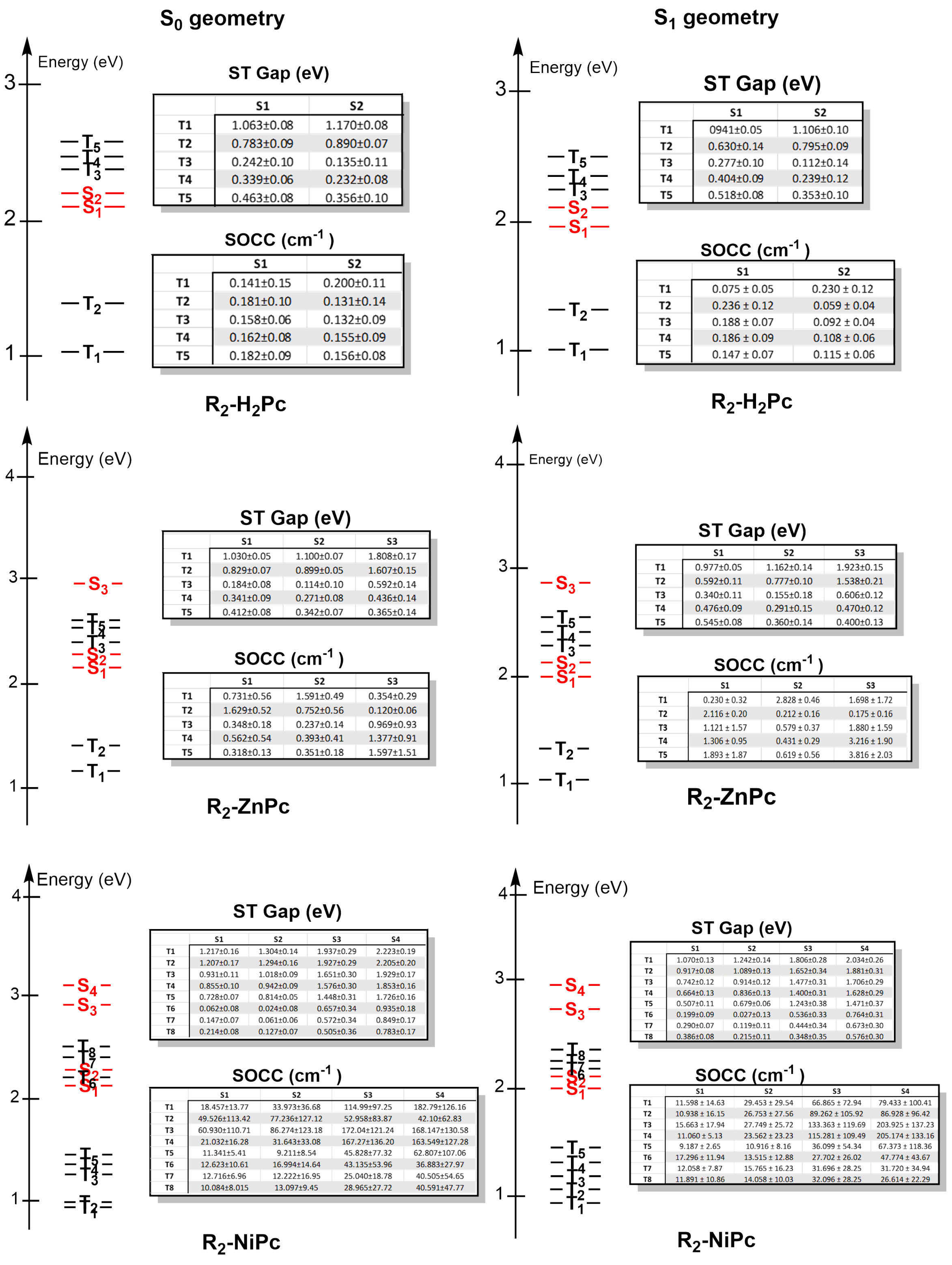

S_0 geometry

ST Gap (eV)

	S1	S2
T1	1.063±0.08	1.170±0.08
T2	0.783±0.09	0.890±0.07
T3	0.242±0.10	0.135±0.11
T4	0.339±0.06	0.232±0.08
T5	0.463±0.08	0.356±0.10

SOCC (cm^{-1})

	S1	S2
T1	0.141±0.15	0.200±0.11
T2	0.181±0.10	0.131±0.14
T3	0.158±0.06	0.132±0.09
T4	0.162±0.08	0.155±0.09
T5	0.182±0.09	0.156±0.08

R_2-H_2Pc

S_1 geometry

ST Gap (eV)

	S1	S2
T1	0941±0.05	1.106±0.10
T2	0.630±0.14	0.795±0.09
T3	0.277±0.10	0.112±0.14
T4	0.404±0.09	0.239±0.12
T5	0.518±0.08	0.353±0.10

SOCC (cm^{-1})

	S1	S2
T1	0.075 ± 0.05	0.230 ± 0.12
T2	0.236 ± 0.12	0.059 ± 0.04
T3	0.188 ± 0.07	0.092 ± 0.04
T4	0.186 ± 0.09	0.108 ± 0.06
T5	0.147 ± 0.07	0.115 ± 0.06

R_2-H_2Pc

ST Gap (eV)

	S1	S2	S3
T1	1.030±0.05	1.100±0.07	1.808±0.17
T2	0.829±0.07	0.899±0.05	1.607±0.15
T3	0.184±0.08	0.114±0.10	0.592±0.14
T4	0.341±0.09	0.271±0.08	0.436±0.14
T5	0.412±0.08	0.342±0.07	0.365±0.14

SOCC (cm^{-1})

	S1	S2	S3
T1	0.731±0.56	1.591±0.49	0.354±0.29
T2	1.629±0.52	0.752±0.56	0.120±0.06
T3	0.348±0.18	0.237±0.14	0.969±0.93
T4	0.562±0.54	0.393±0.41	1.377±0.91
T5	0.318±0.13	0.351±0.18	1.597±1.51

R_2-ZnPc

ST Gap (eV)

	S1	S2	S3
T1	0.977±0.05	1.162±0.14	1.923±0.15
T2	0.592±0.11	0.777±0.10	1.538±0.21
T3	0.340±0.11	0.155±0.18	0.606±0.12
T4	0.476±0.09	0.291±0.15	0.470±0.12
T5	0.545±0.08	0.360±0.14	0.400±0.13

SOCC (cm^{-1})

	S1	S2	S3
T1	0.230 ± 0.32	2.828 ± 0.46	1.698 ± 1.72
T2	2.116 ± 0.20	0.212 ± 0.16	0.175 ± 0.16
T3	1.121 ± 1.57	0.579 ± 0.37	1.880 ± 1.59
T4	1.306 ± 0.95	0.431 ± 0.29	3.216 ± 1.90
T5	1.893 ± 1.87	0.619 ± 0.56	3.816 ± 2.03

R_2-ZnPc

ST Gap (eV)

	S1	S2	S3	S4
T1	1.217±0.16	1.304±0.14	1.937±0.29	2.223±0.19
T2	1.207±0.17	1.294±0.16	1.927±0.29	2.205±0.20
T3	0.931±0.11	1.018±0.09	1.651±0.30	1.929±0.17
T4	0.855±0.10	0.942±0.09	1.576±0.30	1.853±0.16
T5	0.728±0.07	0.814±0.05	1.448±0.31	1.726±0.16
T6	0.062±0.08	0.024±0.08	0.657±0.34	0.935±0.18
T7	0.147±0.07	0.061±0.06	0.572±0.34	0.849±0.17
T8	0.214±0.08	0.127±0.07	0.505±0.36	0.783±0.17

SOCC (cm^{-1})

	S1	S2	S3	S4
T1	18.457±13.77	33.973±36.68	114.99±97.25	182.79±126.16
T2	49.526±113.42	77.236±127.12	52.958±83.87	42.10±62.83
T3	60.930±110.71	86.274±123.18	172.04±121.24	168.147±130.58
T4	21.032±16.28	31.643±33.08	167.27±136.20	163.549±127.28
T5	11.341±5.41	9.211±8.54	45.828±77.32	62.807±107.06
T6	12.623±10.61	16.994±14.64	43.135±53.96	36.883±27.97
T7	12.716±6.96	12.222±16.95	25.040±18.78	40.505±54.65
T8	10.084±8.015	13.097±9.45	28.965±27.72	40.591±47.77

R_2-NiPc

ST Gap (eV)

	S1	S2	S3	S4
T1	1.070±0.13	1.242±0.14	1.806±0.28	2.034±0.26
T2	0.917±0.08	1.089±0.13	1.652±0.34	1.881±0.31
T3	0.742±0.12	0.914±0.12	1.477±0.31	1.706±0.29
T4	0.664±0.13	0.836±0.13	1.400±0.31	1.628±0.29
T5	0.507±0.11	0.679±0.06	1.243±0.38	1.471±0.37
T6	0.199±0.09	0.027±0.13	0.536±0.33	0.764±0.31
T7	0.290±0.07	0.119±0.11	0.444±0.34	0.673±0.30
T8	0.386±0.08	0.215±0.11	0.348±0.35	0.576±0.30

SOCC (cm^{-1})

	S1	S2	S3	S4
T1	11.598 ± 14.63	29.453 ± 29.54	66.865 ± 72.94	79.433 ± 100.41
T2	10.938 ± 16.15	26.753 ± 27.56	89.262 ± 105.92	86.928 ± 96.42
T3	15.663 ± 17.94	27.749 ± 25.72	133.363 ± 119.69	203.925 ± 137.23
T4	11.060 ± 5.13	23.562 ± 23.23	115.281 ± 109.49	205.174 ± 133.16
T5	9.187 ± 2.65	10.916 ± 8.16	36.099 ± 54.34	67.373 ± 118.36
T6	17.296 ± 11.94	13.515 ± 12.88	27.702 ± 26.02	47.774 ± 43.67
T7	12.058 ± 7.87	15.765 ± 16.23	31.696 ± 28.25	31.720 ± 34.94
T8	11.891 ± 10.86	14.058 ± 10.03	32.096 ± 28.25	26.614 ± 22.29

R_2-NiPc

Figure 3.6. Singlet-Triplet Separations (ST Gap) and Spin-Orbit Coupling Constants (SOCC) of R_2Pcs by using geometries of S_0 geometry and S_1 geometry (B3LYP/DZP in water).

4. CONCLUSION

In this thesis, the pentafluorobenzyloxy substituted phthalocyanines and their unsubstituted analogues have been studied as photosensitizer candidates to foresee whether they may be used as light-sensitive drug in photodynamic therapy, DFT and TD-DFT methods have been used to reproduce the absorption features, possible photophysical pathways and excited state topologies.

Ground state geometries are located by using the B3LYP/6-31G* methodology for metal containing complexes, and B3LYP/6-311G** methodology for the others. The coordinating metal atom slightly effects the phthalocyanine geometry, especially the width of the cavity is dependent on the size of atom.

In this study, two different approaches are used methodologically: static and dynamic. The results draw attention to the importance of including vibrational effects to predict more reliable photophysical properties of the molecules. The band shapes are obtained more realistic by using the randomly generated geometries by sampling the ground state and excited state geometries based on the Wigner distribution function. The vertical transitions, calculated by ωB97XD/6-311G**, are strongly dependent on the solvent environment. Since the PS is injected to a water-based environment, the absorbances of R_1-H_2Pc, R_1-NiPc, R_2-H_2Pc and R_2-NiPc are red shifted in water phase compared to those in vacuum phase. On the other hand, R_1-ZnPc and R_2-ZnPc exhibit blue shift in water phase. The emission properties of molecules are calculated by using the ωB97XD/6-31G* methodology. Based on the NTO results, the pentafluorobenzyloxy substituent has almost no influence on excite state properties of the R_2Pcs, the substituent is probably used to reduce the aggregation formation due to π-π stacking.

R_1-Pcs and R_2-Pcs have absorbance in the near-infrared region, which is a precaution for being suitable drug for photodynamic therapy. Moreover, R_1-H_2Pc, R_1-ZnPc, R_2-H_2Pc and R_2-ZnPc may be used as photosensitizers to diagnose malignant cells. However, such applications would require some other additional properties such as not having any toxicity, that is beyond the scope of this study.

The studied molecules are able to populate their triplet states. The intersystem crossing probability is strongly dependent on their spin-orbit coupling constants (SOCC) and singlet triplet separations (Δ_{ST}), by calculating SOCC and Δ_{ST}, the possible ISC pathways are elucidated. All of them prefer to follow the indirect mechanism to populate the triplet state. However, R_1-NiPc and R_2-NiPc are not capable of producing singlet oxygen since their populated T_1 state is below the treshold energy (0.98 eV).

This study clarifies that the photophysical properties of R_1-H_2Pc, R_1-ZnPc, R_2-H_2Pc and R_2-ZnPc are satisfactory to be used as photosensitizer in photodynamic therapy. However, the aggregation is usually a problem for photosensitizing applications of phthalocyanine compounds due to interactions between chains such as π-π stacking, hydrogen bonding, ligand-metal coordination and donor-acceptor interactions. The efficiency of the therapy is severely influenced since the aggregates reduce the singlet oxygen quantum yield and decrease the triplet life-time. Therefore, the aggregation behavior is another predominant reason to influence the therapy efficiency. In the future, the dimer and trimer structures of the selected ones in body environment should be taken into account to predict the photosensitizer's efficiency in the therapy.

REFERENCES

1. Pedersen, C. J., "The discovery of crown ethers", *Science (80-.).*, Vol. 241, No. 4865, pp. 536–540, July 1988.
2. Jones, R. D., D. A. Summerville and F. Basolo, "Synthetic Oxygen Carriers Related to Biological Systems", *Chem. Rev.*, 1979.
3. Randic, M., "Aromaticity and conjugation", *J. Am. Chem. Soc.*, Vol. 99, No. 2, pp. 444–450, January 1977.
4. Lenzoff, C. and A. Lever, *Phthalocyanines : properties and applications. Volume 4*, VCH, 1996.
5. de Diesbach, H. and E. von der Weid, "Quelques sels complexes des o-dinitriles avec le cuivre et la pyridine", *Helv. Chim. Acta*, Vol. 10, No. 1, pp. 886–888, January 1927.
6. Gregory, P., "Steamrollers, Sports Cars and Security: Phthalocyanine Progress Through the Ages", *J. Porphyrins Phthalocyanines*, 1999.
7. Gregory, P., "Industrial applications of phthalocyanines", *J. Porphyr. Phthalocyanines*, Vol. 4, pp. 432–437, Wiley-Blackwell, June 2000.
8. Barrett, P. A., D. A. Frye and R. P. Linstead, "213. Phthalocyanines and associated compounds. Part XIV. Further investigations of metallic derivatives", *J. Chem. Soc.*, 1938.
9. Linstead, R. P. and A. R. Lowe, "216. Phthalocyanines. Part V. The molecular weight of magnesium phthalocyanine", *J. Chem. Soc.*, Vol. 0, No. 0, p. 1031, January 1934.

10. Dent, C. E., R. P. Linstead and A. R. Lowe, "217. Phthalocyanines. Part VI. The structure of the phthalocyanines", *J. Chem. Soc.*, Vol. 0, No. 0, p. 1033, January 1934.

11. Linstead, R. P., "212. Phthalocyanines. Part I. A new type of synthetic colouring matters", *J. Chem. Soc.*, Vol. 0, No. 0, p. 1016, January 1934.

12. Dent, C. E. and R. P. Linstead, "215. Phthalocyanines. Part IV. Copper phthalocyanines", *J. Chem. Soc.*, Vol. 0, No. 0, p. 1027, January 1934.

13. Linstead, R. P. and A. R. Lowe, "214. Phthalocyanines. Part III. Preliminary experiments on the preparation of phthalocyanines from phthalonitrile", *J. Chem. Soc.*, Vol. 0, No. 0, p. 1022, January 1934.

14. Sharman, W. M. and J. E. Van Lier, "Synthesis of Phthalocyanine Precursors", *Porphyr. Handb. Phthalocyanines Synth.*, 2012.

15. Erk, P. and H. Hengelsberg, "Phthalocyanine Dyes and Pigments", *Porphyr. Handb. Multporphyrins, Multiphthalocyanines Arrays*, 2012.

16. Robertson, J. M., "136. An X-ray study of the structure of the phthalocyanines. Part I. The metal-free, nickel, copper, and platinum compounds", *J. Chem. Soc.*, 1935.

17. Boucher, L. J., "Metal Complexes of Phthalocyanines", *Coord. Chem. Macrocycl. Compd.*, pp. 461–516, Springer US, Boston, MA, 1979.

18. Jiang, J. and K. P. N. G. Dennis, "A decade journey in the chemistry of sandwich-type tetrapyrrolato-rare earth complexes", *Acc. Chem. Res.*, Vol. 42, No. 1, pp. 79–88, January 2009.

19. Cuellar, E. A. and T. J. Marks, "Synthesis and Characterization of Metallo and Metal-Free Octaalkylphthalocyanines and Uranyl Decaalkylsuperphthalocya-

nines", *Inorg. Chem.*, Vol. 20, No. 11, pp. 3766–3770, 1981.

20. Ohno-Okumura, E., K. Sakamoto, T. Kato, T. Hatano, K. Fukui, T. Karatsu, A. Kitamura and T. Urano, "Synthesis of subphthalocyanine derivatives and their characterization", *Dye. Pigment.*, Vol. 53, No. 1, pp. 57–65, April 2002.

21. Kadish, K. M., K. M. Smith and R. Guilard, *Phthalocyanines : properties and materials*, Academic Press, 2003.

22. Maya, E. M., A. W. Snow, J. S. Shirk, R. G. Pong, S. R. Flom and G. L. Roberts, "Synthesis, aggregation behavior and nonlinear absorption properties of lead phthalocyanines substituted with siloxane chains", *J. Mater. Chem.*, Vol. 13, No. 7, pp. 1603–1613, 2003.

23. Tuncer, S., K. Kaya, b. Özçeşmeci and A. K. Burat, "Non-peripherally tetrasubstituted phthalocyanines: Synthesis, characterization and, photophysical investigation", *J. Organomet. Chem.*, Vol. 827, pp. 78–85, January 2017.

24. Özçeşmeci, M., I. B. Özçeşmeci and E. Hamuryudan, "Synthesis and characterization of new polyfluorinated dendrimeric phthalocyanines", *Polyhedron*, Vol. 29, No. 13, pp. 2710–2715, 2010.

25. Özçeşmeci, I., A. Tekin and A. Gül, "Synthesis and aggregation behavior of zinc phthalocyanines substituted with bulky naphthoxy and phenylazonaphthoxy groups: An experimental and theoretical study", *Synth. Met.*, Vol. 189, pp. 100–110, March 2014.

26. Karaoğlu, H. R., A. Koca and M. B. Koçak, "Synthesis, electrochemical and spectroelectrochemical characterization of novel soluble phthalocyanines bearing chloro and quaternizable bulky substituents on peripheral positions", *Dye. Pigment.*, Vol. 92, No. 3, pp. 1005–1017, March 2012.

27. Atsay, A., A. Gül and M. Burkut Koçak, "A new hexadeca substituted non-

aggregating zinc phthalocyanine", *Dye. Pigment.*, Vol. 100, pp. 177–183, January 2014.

28. Ghani, F., J. Kristen and H. Riegler, "Solubility properties of unsubstituted metal phthalocyanines in different types of solvents", *J. Chem. Eng. Data*, Vol. 57, No. 2, pp. 439–449, February 2012.

29. Lever, A. B., S. R. Pickens, P. C. Minor, S. Licoccia, B. S. Ramaswamy and K. Magnell, "Charge-Transfer Spectra of Metallophthalocyanines: Correlation with Electrode Potentials", *J. Am. Chem. Soc.*, Vol. 103, No. 23, pp. 6800–6806, November 1981.

30. Lever, A. B., "The Phthalocyanines", *Adv. Inorg. Chem. Radiochem.*, Vol. 7, No. C, pp. 27–114, January 1965.

31. Claessens, C. G., U. Hahn and T. Torres, "Phthalocyanines: From outstanding electronic properties to emerging applications", *Chem. Rec.*, Vol. 8, No. 2, pp. 75–97, 2008.

32. Schaffer, A. M. and M. Gouterman, "Porphyrins XXV. Extended Hückel calculations on location and spectral effects of free base protons", *Theor. Chim. Acta*, Vol. 25, No. 1, pp. 62–82, 1972.

33. Schaffer, A. M., M. Gouterman and E. R. Davidson, "Porphyrins XXVIII. Extended Hückel calculations on metal phthalocyanines and tetrazaporphins", *Theor. Chim. Acta*, Vol. 30, No. 1, pp. 9–30, 1973.

34. Edwards, L. and M. Gouterman, "Porphyrins. XV. Vapor absorption spectra and stability: Phthalocyanines", *J. Mol. Spectrosc.*, Vol. 33, No. 2, pp. 292–310, February 1970.

35. McHugh, A. J., M. Gouterman and C. Weiss, "Porphyrins XXIV. Energy, oscillator strength, and Zeeman splitting calculations (SCMO-CI) for phthalocyanine,

porphyrins, and related ring systems", *Theor. Chim. Acta*, Vol. 24, No. 4, pp. 346–370, December 1972.

36. Heilmeier, G. H. and G. Warfield, "Optical Absorption Spectrum of Metal Free Phthalocyanine Single Crystals", *J. Chem. Phys.*, Vol. 38, No. 4, pp. 893–897, 1963.

37. Saka, E. T., C. Göl, M. Durmuş, H. Kantekin and Z. Biyiklioglu, "Photophysical, photochemical and aggregation behavior of novel peripherally tetra-substituted phthalocyanine derivatives", *J. Photochem. Photobiol. A Chem.*, Vol. 241, pp. 67–78, 2012.

38. Yanik, H., D. Aydin, M. Durmuş and V. Ahsen, "Peripheral and non-peripheral tetrasubstituted aluminium, gallium and indium phthalocyanines: Synthesis, photophysics and photochemistry", *J. Photochem. Photobiol. A Chem.*, Vol. 206, No. 1, pp. 18–26, July 2009.

39. Ishikawa, N., "Electronic structures and spectral properties of double- and triple-decker phthalocyanine complexes in a localized molecular orbital view", *J. Porphyr. Phthalocyanines*, Vol. 5, No. 1, pp. 87–101, January 2001.

40. Benihya, K., M. Mossoyan-Déneux, F. Hahn, N. Boucharat and G. Terzian, "Synthesis, Crystal Structure and Spectral Characterization, of a New Phase of Tris(phthalocyaninato)dibismuth(III), Bi2(Pc)3", *Eur. J. Inorg. Chem.*, Vol. 2000, No. 8, pp. 1771–1779, August 2000.

41. Javier Ramos, F., M. Ince, M. Urbani, A. Abate, M. Grätzel, S. Ahmad, T. Torres and M. K. Nazeeruddin, "Non-aggregated Zn(ii)octa(2,6-diphenylphenoxy) phthalocyanine as a hole transporting material for efficient perovskite solar cells", *Dalt. Trans.*, Vol. 44, No. 23, pp. 10847–10851, June 2015.

42. Yanık, H., S. Yeşilot and M. Durmuş, "Synthesis and properties of octa-distyryl-BODIPY substituted zinc(II) phthalocyanines", *Dye. Pigment.*, Vol. 140, pp. 157–

165, May 2017.

43. Mu, B., K. Chen, J. Chen, J. Fang and D. Chen, "Toward well-organised ionic discotic liquid crystals via versatile supramolecular approach", *Liq. Cryst.*, Vol. 45, No. 9, pp. 1287–1293, July 2018.

44. Zhang, Y., X. Cai, Y. Bian and J. Jiang, "Organic semiconductors of phthalocyanine compounds for field effect transistors (FETs)", *Struct. Bond.*, Vol. 135, pp. 275–322, 2010.

45. Izaki, M., R. Chizaki, T. Saito, K. Murata, J. Sasano and T. Shinagawa, "Hybrid ZnO/phthalocyanine photovoltaic device with highly resistive ZnO intermediate layer", *ACS Appl. Mater. Interfaces*, Vol. 5, No. 19, pp. 9386–9395, October 2013.

46. Bohrer, F. I., A. Sharoni, C. Colesniuc, J. Park, I. K. Schuller, A. C. Kummel and W. C. Trogler, "Gas sensing mechanism in chemiresistive cobalt and metal-free phthalocyanine thin films", *J. Am. Chem. Soc.*, Vol. 129, No. 17, pp. 5640–5646, 2007.

47. Bohrer, F. I., C. N. Colesniuc, J. Park, M. E. Ruidiaz, I. K. Schuller, A. C. Kummel and W. C. Trogler, "Comparative gas sensing in cobalt, nickel, copper, zinc, and metal-free phthalocyanine chemiresistors", *J. Am. Chem. Soc.*, Vol. 131, No. 2, pp. 478–485, 2009.

48. Zhu, M., R. Ye, K. Jin, N. Lazouski and K. Manthiram, "Elucidating the Reactivity and Mechanism of CO2Electroreduction at Highly Dispersed Cobalt Phthalocyanine", *ACS Energy Lett.*, Vol. 3, No. 6, pp. 1381–1386, 2018.

49. Qian, Y., Z. Liu, H. Zhang, P. Wu and C. Cai, "Active Site Structures in Nitrogen-Doped Carbon-Supported Cobalt Catalysts for the Oxygen Reduction Reaction", *ACS Appl. Mater. Interfaces*, Vol. 8, No. 48, pp. 32875–32886, December 2016.

50. Li, X., H. Wang and H. Wu, "Phthalocyanines and their analogs applied in dye-

sensitized solar cell", *Struct. Bond.*, Vol. 135, pp. 229–274, 2010.

51. Fischer, M. K., I. López-Duarte, M. M. Wienk, M. V. Martínez-Díaz, R. A. Janssen, P. Bäuerle and T. Torres, "Functionalized dendritic oligothiophenes: Ruthenium phthalocyanine complexes and their application in bulk heterojunction solar cells", *J. Am. Chem. Soc.*, Vol. 131, No. 24, pp. 8669–8676, June 2009.

52. Hasrat, A. and J. E. van Lier, "Phthalocyanines in Cancer-Imaging and Therapy", *Handb. Photodyn. Ther. Updat. Recent Appl. Porphyrin-Based Compd.*, pp. 173–235, World Scientific, June 2016.

53. Cyza, M., A. Gut, Ł. Łapok, J. Solarski, V. Knyukshto, M. Kępczyński and M. Nowakowska, "Iodinated zinc phthalocyanine – The novel visible-light activated photosensitizer for efficient generation of singlet oxygen", *J. Photochem. Photobiol. A Chem.*, Vol. 358, pp. 265–273, May 2018.

54. Lo, C. S., P.C. and D. Ng, "Molecular Phthalocyanine-Based Photosensitizers for Photodynamic Therapy", *Handb. Photodyn. Ther. Updat. Recent Appl. Porphyrin-Based Compd.*, pp. 237–272, World Scientific, June 2016.

55. Mather, R. R., "The Effect of Crystal Properties on the Manufacture and Application Performance of Copper Phthalocyanine Pigments", *J. Porphyrins Phthalocyanines*, Vol. 03, No. 07, pp. 643–646, October 1999.

56. Tianyong, Z. and Z. Chunlong, "Properties of copper phthalocyanine blue (C.I. Pigment Blue 15:3) treated with poly(ethylene glycol)s", *Dye. Pigment.*, Vol. 35, No. 2, pp. 123–130, October 1997.

57. García-Iglesias, M., J.-H. Yum, R. Humphry-Baker, S. M. Zakeeruddin, P. Péchy, P. Vázquez, E. Palomares, M. Grätzel, M. K. Nazeeruddin and T. Torres, "Effect of anchoring groups in zinc phthalocyanine on the dye-sensitized solar cell performance and stability", *Chem. Sci.*, Vol. 2, No. 6, p. 1145, 2011.

58. Organization, W. H., *Cancer, Factsheet N°297*, accessed at December 2018.

59. Majumdar, P., R. Nomula and J. Zhao, “Activatable triplet photosensitizers: magic bullets for targeted photodynamic therapy”, *J. Mater. Chem. C*, Vol. 2, No. 30, pp. 5982–5997, 2014.

60. Fass, L., “Imaging and cancer: A review”, *Molecular Oncology*, Vol. 2, No. 2, pp. 115 – 152, 2008.

61. Yuan, L., W. Lin, K. Zheng, L. He and W. Huang, “Far-red to near infrared analyte-responsive fluorescent probes based on organic fluorophore platforms for fluorescence imaging”, *Chem. Soc. Rev.*, Vol. 42, No. 2, pp. 622–661, December 2013.

62. Maity, D. and T. Govindaraju, “A turn-on NIR fluorescence and colourimetric cyanine probe for monitoring the thiol content in serum and the glutathione reductase assisted glutathione redox process”, *Org. Biomol. Chem.*, Vol. 11, No. 13, p. 2098, March 2013.

63. Yokoi, T., T. Otani and K. Ishii, “In vivo fluorescence bioimaging of ascorbic acid in mice: Development of an efficient probe consisting of phthalocyanine, Tempo, and Albumin”, *Sci. Rep.*, Vol. 8, No. 1, p. 1560, December 2018.

64. Kepczynski, M., M. Dzieciuch and M. Nowakowska, “Nanostructural hybrid sensitizers for photodynamic therapy”, *Curr. Pharm. Des.*, Vol. 18, No. 18, pp. 2607–2621, April 2012.

65. Ormond, A. B. and H. S. Freeman, “Dye sensitizers for photodynamic therapy”, *Materials (Basel).*, Vol. 6, No. 3, pp. 817–840, 2013.

66. Bott, T., “Basic Principles”, R. Pottier, B. Krammer, H. Stepp and R. Baumgartner (Editors), *Fouling Heat Exch.*, pp. 7–14, October 1995.

67. Henderson, B. W. and T. J. Dougherty, “How Does Photodynamic Therapy Work?”, *Photochemistry and Photobiology*, Vol. 55, No. 1, pp. 145–157, 1992.

68. Poli, R. and J. N. Harvey, “Spin forbidden chemical reactions of transition metal compounds. New ideas and new computational challenges”, *Chem. Soc. Rev.*, Vol. 32, pp. 1–8, 2003.

69. Gomer, C. J., A. Ferrario, N. Hayashi, N. Rucker, B. C. Szirth and A. L. Murphree, “Molecular, cellular, and tissue responses following photodynamic therapy”, *Lasers Surg. Med.*, Vol. 8, No. 5, pp. 450–463, January 1988.

70. Gomer, C. J., “Preclinical Examination of First and Second Generation Photosensitizers Used in Photodynamic Therapy”, *Photochemistry and Photobiology*, Vol. 54, No. 6, pp. 1093–1107, 1991.

71. de Souza, T. G. B., M. G. Vivas, C. R. Mendonça, S. Plunkett, M. A. Filatov, M. O. Senge and L. De Boni, “Studying the intersystem crossing rate and triplet quantum yield of meso-substituted porphyrins by means of pulse train fluorescence technique”, *J. Porphyr. Phthalocyanines*, Vol. 20, No. 01n04, pp. 282–291, 2016.

72. DeRosa, M. C. and R. J. Crutchley, “Photosensitized singlet oxygen and its applications”, *Coord. Chem. Rev.*, Vol. 233-234, pp. 351–371, 2002.

73. Abrahamse, H. and M. R. Hamblin, “New photosensitizers for photodynamic therapy”, *Biochemical Journal*, Vol. 473, No. 4, pp. 347–364, 2016.

74. Lanzo, I., A. D. Quartarolo, N. Russo and E. Sicilia, “Can subpyriporphyrin and its boron complex be proposed as photosensitizers in photodynamic therapy ? A first principle time dependent study.”, *Photochem. Photobiol. Sci.*, Vol. 8, No. 3, pp. 386–390, 2009.

75. Arnold, R., “Dyes and Pigments. New Research”, *Nova Science Publishers*, 2010.

76. Moreira, L. M., F. V. Dos Santos, J. P. Lyon, M. Maftoum-Costa, C. Pacheco-Soares and N. Soares Da Silva, "Photodynamic therapy: Porphyrins and phthalocyanines as photosensitizers", *Aust. J. Chem.*, Vol. 61, No. 10, pp. 741–754, October 2008.

77. Dougherty, T. J., M. T. Cooper and T. S. Mang, "Cutaneous phototoxic occurrences in patients receiving Photofrin®", *Lasers Surg. Med.*, Vol. 10, No. 5, pp. 485–488, January 1990.

78. Wöhrle, D., A. Hirth, T. Bogdahn-Rai, G. Schnurpfeil and M. Shopova, "Photodynamic therapy of cancer: Second and third generations of photosensitizers", *Russ. Chem. Bull.*, Vol. 47, No. 5, pp. 807–816, May 1998.

79. Baptista, M. S., J. Cadet, P. Di Mascio, A. A. Ghogare, A. Greer, M. R. Hamblin, C. Lorente, S. C. Nunez, M. S. Ribeiro, A. H. Thomas, M. Vignoni and T. M. Yoshimura, "Type I and Type II Photosensitized Oxidation Reactions: Guidelines and Mechanistic Pathways", *Photochemistry and Photobiology*, Vol. 93, No. 4, pp. 912–919.

80. Rajendran, M., "Quinones as photosensitizer for photodynamic therapy: ROS generation, mechanism and detection methods", *Photodiagnosis and Photodynamic Therapy*, Vol. 13, pp. 175 – 187, 2016.

81. Xodo, L. E., Susanna, Cogoi1 and &. V. Rapozzi, "Photosensitizers binding to nucleic acids as anticancer agents", *Future Med. Chem.*, Vol. 8, No. 2, p. 712, February 2010.

82. Menezes, P. F., V. S. Bagnato, R. M. Johnke, C. Bonnerup, C. H. Sibata, R. R. Allison and J. R. Perussi, "Photodynamic therapy for Photogem® and Photofrin® using different light wavelengths in 375 human melanoma cells", *Laser Phys. Lett.*, Vol. 4, No. 7, pp. 546–551, July 2007.

83. Allison, R. R. and C. H. Sibata, "Oncologic photodynamic therapy photosensitiz-

ers: A clinical review", *Photodiagnosis and Photodynamic Therapy*, Vol. 7, No. 2, pp. 61 – 75, 2010.

84. Selçukoğlu, M. and E. Hamuryudan, "Novel phthalocyanines with pentafluorobenzyloxy-substituents", *Dye. Pigment.*, Vol. 74, No. 1, pp. 17–20, January 2007.

85. Loeb, A. L., "The Heisenberg Uncertainty Principle", *Am. J. Phys.*, Vol. 31, No. 12, p. 945, 1963.

86. Born, M. and R. Oppenheimer, "Zur Quantentheorie der Molekeln", *Ann. Phys.*, Vol. 389, No. 20, pp. 457–484, January 1927.

87. Engel, E. and R. M. Dreizler, "Density Functional Theory: An Advanced Course", *Theor. Math. Phys.*, Vol. 2011, No. 5, pp. 499–515, 2011.

88. Becke, A. D., "A new mixing of Hartree-Fock and local density-functional theories", *J. Chem. Phys.*, Vol. 98, No. 2, pp. 1372–1377, January 1993.

89. Becke, A. D., "Density-functional exchange-energy approximation with correct asymptotic behavior", *Phys. Rev. A*, Vol. 38, No. 6, pp. 3098–3100, September 1988.

90. Hohenberg, P. and W. Kohn, "Inhomogeneous Electron Gas", *Phys. Rev.*, Vol. 136, pp. B864–B871, November 1964.

91. Kohn, W. and L. J. Sham, "Self-consistent equations including exchange and correlation effects", *Phys. Rev.*, Vol. 140, No. 4A, pp. A1133–A1138, November 1965.

92. Leach, A. R., *Molecular modelling : principles and applications*, Prentice Hall, 2001.

93. Perdew, J. P., K. Burke and M. Ernzerhof, "Generalized gradient approximation

made simple", *Phys. Rev. Lett.*, Vol. 77, No. 18, pp. 3865–3868, October 1996.

94. Lee, C., W. Yang and R. G. Parr, "Development of the Colle-Salvetti correlation-energy formula into a functional of the electron density", *Phys. Rev. B*, Vol. 37, No. 2, pp. 785–789, 1988.

95. Pauling, L., "The nature of the chemical bond. IV. The energy of single bonds and the relative electronegativity of atoms", *J. Am. Chem. Soc.*, Vol. 54, No. 9, pp. 3570–3582, September 1932.

96. Vydrov, O. A. and G. E. Scuseria, "Assessment of a long-range corrected hybrid functional", *The Journal of Chemical Physics*, Vol. 125, No. 23, p. 234109, 2006.

97. Chai, J. D. and M. Head-Gordon, "Long-range corrected hybrid density functionals with damped atom-atom dispersion corrections", *Phys. Chem. Chem. Phys.*, Vol. 10, No. 44, pp. 6615–6620, 2008.

98. Slater, J. C., "Atomic shielding constants", *Phys. Rev.*, Vol. 36, No. 1, pp. 57–64, July 1930.

99. Boys, S. F., "Electronic Wave Functions. I. A General Method of Calculation for the Stationary States of Any Molecular System", *Proc. R. Soc. A Math. Phys. Eng. Sci.*, Vol. 200, No. 1063, pp. 542–554, 1950.

100. Miertuš, S., E. Scrocco and J. Tomasi, "Electrostatic interaction of a solute with a continuum. A direct utilizaion of AB initio molecular potentials for the prevision of solvent effects", *Chem. Phys.*, Vol. 55, No. 1, pp. 117–129, February 1981.

101. Runge, E. and E. K. U. Gross, "Density-Functional Theory for Time-Dependent Systems", *Phys. Rev. Lett.*, Vol. 52, pp. 997–1000, March 1984.

102. Wigner, E. P., "On the Quantum Correction for Thermodynamic Equilibrium", *Part I Phys. Chem. Part II Solid State Phys.*, pp. 110–120, Springer Berlin Hei-

delberg, Berlin, Heidelberg, 1997.

103. Steuernagel, O., D. Kakofengitis and G. Ritter, “Wigner flow reveals topological order in quantum phase space dynamics”, *Phys. Rev. Lett.*, Vol. 110, No. 3, 2013.

104. Zobel, J. P., M. Heindl, J. J. Nogueira and L. González, “Vibrational Sampling and Solvent Effects on the Electronic Structure of the Absorption Spectrum of 2-Nitronaphthalene”, *J. Chem. Theory Comput.*, Vol. 14, No. 6, pp. 3205–3217, 2018.

105. Etienne, T., X. Assfeld and A. Monari, “Toward a quantitative assessment of electronic transitions” charge-transfer character”, *J. Chem. Theory Comput.*, Vol. 10, No. 9, pp. 3896–3905, September 2014.

106. Lee, C., W. Yang and R. G. Parr, “Development of the Colle-Salvetti correlation-energy formula into a functional of the electron density”, *Phys. Rev. B*, Vol. 37, No. 2, pp. 785–789, January 1988.

107. Frisch, M. J., G. W. Trucks, H. B. Schlegel, G. E. Scuseria, M. A. Robb, J. R. Cheeseman and G. S. et al., “Gaussian 09 Revision E.01”, Gaussian Inc. Wallingford CT, 2009.

108. Tomasi, J. and M. Persico, “Molecular Interactions in Solution: An Overview of Methods Based on Continuous Distributions of the Solvent”, *Chem. Rev.*, Vol. 94, No. 7, pp. 2027–2094, November 1994.

109. Schinke, R., *Photodissociation Dynamics: Spectroscopy and Fragmentation of Small Polyatomic Molecules*, Cambridge University Press, 1993.

110. Dahl, J. P. and M. Springborg, “The Morse oscillator in position space, momentum space, and phase space”, *J. Chem. Phys.*, Vol. 88, No. 7, pp. 4535–4547, 1988.

111. Barbatti, M., M. Ruckenbauer, F. Plasser, J. Pittner, G. Granucci, M. Persico and H. Lischka, "Newton-X: A surface-hopping program for nonadiabatic molecular dynamics", *Wiley Interdiscip. Rev. Comput. Mol. Sci.*, Vol. 4, No. 1, pp. 26–33, 2014.

112. Etienne, T., "Probing the locality of excited states with linear algebra", *J. Chem. Theory Comput.*, Vol. 11, No. 4, pp. 1692–1699, April 2015.

113. Etienne, T., X. Assfeld and A. Monari, "New insight into the topology of excited states through detachment/attachment density matrices-based centroids of charge", *J. Chem. Theory Comput.*, Vol. 10, No. 9, pp. 3906–3914, September 2014.

114. Velde, G., F. M. Bickelhaupt, S. J. A. van Gisbergen, C. F. Guerra, E. J. Baerends, J. G. Snijders and T. Ziegler, "Chemsitry with ADF", *J. Comput. Chem.*, Vol. 22, No. 9, p. 931, 2001.

115. Fonseca Guerra, C., J. G. Snijders, G. Te Velde and E. J. Baerends, "Towards an order-N DFT method", *Theor. Chem. Acc.*, Vol. 99, No. 6, pp. 391–403, November 1998.

116. Van Lenthe, E. and E. J. Baerends, "Optimized Slater-type basis sets for the elements 1-118", *J. Comput. Chem.*, Vol. 24, No. 9, pp. 1142–1156, July 2003.

117. Li, L., Q. Tang, H. Li, X. Yang, W. Hu, Y. Song, Z. Shuai, W. Xu, Y. Liu and D. Zhu, "An ultra closely π-stacked organic semiconductor for high performance field-effect transistors", *Adv. Mater.*, Vol. 19, No. 18, pp. 2613–2617, September 2007.

118. Scheidt, W. R. and W. Dow, "Molecular Stereochemistry of Phthalocyanatozinc(II)", *J. Am. Chem. Soc.*, Vol. 99, No. 4, pp. 1101–1104, February 1977.

119. Nguyen, K. A., P. N. Day and R. Pachter, "Effects of halogenation on the ionized

and excited states of free-base and zinc porphyrins", *J. Chem. Phys.*, Vol. 110, No. 18, pp. 9135–9144, April 1999.

120. Robertson, J. M., "136. An X-ray study of the structure of the phthalocyanines. Part I. The metal-free, nickel, copper, and platinum compounds", *J. Chem. Soc.*, pp. 615–621, 1935.

121. Selçukoğlu, M., *Fluorlu Gruplar İçeren Ftalosiyaninler.*, Fen Bilimleri Enstitüsü, 2005.

122. Regehly, M., K. Greish, F. Rancan, H. Maeda, F. Böhm and B. Röder, "Water-soluble polymer conjugates of ZnPP for photodynamic tumor therapy", *Bioconjug. Chem.*, Vol. 18, No. 2, pp. 494–499, 2007.

123. Zhang, P., W. Steelant, M. Kumar and M. Scholfield, "Versatile photosensitizers for photodynamic therapy at infrared excitation", *J. Am. Chem. Soc.*, Vol. 129, No. 15, pp. 4526–4527, 2007.

124. McDonnell, S. O., M. J. Hall, L. T. Allen, A. Byrne, W. M. Gallagher and D. F. O'Shea, "Supramolecular photonic therapeutic agents", *J. Am. Chem. Soc.*, Vol. 127, No. 47, pp. 16360–16361, 2005.

125. Nyman, E. S. and P. H. Hynninen, "Research advances in the use of tetrapyrrolic photosensitizers for photodynamic therapy", *Journal of Photochemistry and Photobiology B: Biology*, Vol. 73, No. 1, pp. 1 – 28, 2004.

126. Chen, B., B. W. Pogue, X. Zhou, J. A. O'Hara, N. Solban, E. Demidenko, P. J. Hoopes and T. Hasan, "Effect of tumor host microenvironment on photodynamic therapy in a rat prostate tumor model", *Clin. Cancer Res.*, Vol. 11, No. 2 I, pp. 720–727, June 2005.

127. Barentsz, J. O., M. Engelbrecht, G. J. Jager, J. A. Witjes, J. de LaRosette, B. P. van der Sanden, H.-J. Huisman and A. Heerschap, "Fast dynamic gadolinium-

enhanced MR imaging of urinary bladder and prostate cancer", *J. Magn. Reson. Imaging*, Vol. 10, No. 3, pp. 295–304, September 1999.

128. Hsiao, H.-P., L. S. Kirschner, I. Bourdeau, M. F. Keil, S. A. Boikos, S. Verma, A. J. Robinson-White, M. Nesterova, A. Lacroix and C. A. Stratakis, "Clinical and Genetic Heterogeneity, Overlap with Other Tumor Syndromes, and Atypical Glucocorticoid Hormone Secretion in Adrenocorticotropin-Independent Macronodular Adrenal Hyperplasia Compared with Other Adrenocortical Tumors", *J. Clin. Endocrinol. Metab.*, Vol. 94, No. 8, pp. 2930–2937, August 2009.

129. Pirillo, J., G. Mazzone and N. Russo, "Theoretical Insights into the Switching Off/On of 1O2 Photosensitization in Chemicontrolled Photodynamic Therapy", *Chem. - A Eur. J.*, Vol. 24, No. 14, pp. 3512–3519, March 2018.

130. Mai, S., P. Marquetand and L. González, "Intersystem Crossing Pathways in the Noncanonical Nucleobase 2-Thiouracil: A Time-Dependent Picture", *The Journal of Physical Chemistry Letters*, Vol. 7, No. 11, pp. 1978–1983, 2016, pMID: 27167106.

131. Marian, C. M., "Spin–orbit coupling and intersystem crossing in molecules", *Wiley Interdisciplinary Reviews: Computational Molecular Science*, Vol. 2, No. 2, pp. 187–203.

132. Sengul, O., M. Marazzi, A. Monari and S. Catak, "Photophysical Properties of Novel Two-Photon Absorbing Dyes: Assessing Their Possible Use for Singlet Oxygen Generation", *The Journal of Physical Chemistry C*, Vol. 122, No. 28, pp. 16315–16324, 2018.